Biol. Cybern. 84, 365–382 (2001)

Biological Cybernetics

Stable operation of an elastic three-segment leg

André Seyfarth, Michael Günther, Reinhard Blickhan

Institute of Sports Science, Friedrich-Schiller University, Seidelstr. 20, 07749 Jena, Germany

Abstract. Quasi-elastic operation of joints in multi-segmented systems as they occur in the legs of humans, animals, and robots requires a careful tuning of leg properties and geometry if catastrophic counteracting operation of the joints is to be avoided. A simple three-segment model has been used to investigate the segmental organization of the leg during repulsive tasks like human running and jumping. The effective operation of the muscles crossing the knee and ankle joints is described in terms of rotational springs. The following issues were addressed in this study: (1) how can the joint torques be controlled to result in a spring-like leg operation? (2) how can rotational stiffnesses be adjusted to leg-segment geometry? and (3) to what extend can unequal segment lengths and orientations be advantageous? It was found that: (1) the three-segment leg tends to become unstable at a certain amount of bending expressed by a counter-rotation of the joints; (2) homogeneous bending requires adaptation of the rotational stiffnesses to the outer segment lengths; (3) nonlinear joint torque-displacement behaviour extends the range of stable leg bending and may result in an almost constant leg stiffness; (4) biarticular structures (like human gastrocnemius muscle) and geometrical constraints (like heel strike) support homogeneous bending in both joints; (5) unequal segment lengths enable homogeneous bending if asymmetric nominal angles meet the asymmetry in leg geometry; and (6) a short foot supports the elastic control of almost stretched knee positions. Furthermore, general leg design strategies for animals and robots are discussed with respect to the range of safe leg operation.

1 Introduction

Although many movement studies using the leg-spring concept can be found in the literature (Blickhan 1989; Farley and González 1996; Seyfarth et al. 1999), little is known about the mechanisms and benefits of such a manner of leg operation. The concept of spring-like operation of the total leg can be extended to spring-like operation of joints for exercises such as hopping, running, and jumping (Stefanyshyn and Nigg 1998; Farley and Morgenroth 1999). Depending on the execution characteristics, exhaustion or external constraints changes in joint kinetics and kinematics have been observed (e.g., Williams et al. 1991; Farley et al. 1998; Kovács et al. 1999). Thereby the elastic operation of joints may disappear depending on movement criteria such as foot placement (Kovács et al. 1999) or hopping height (Farley and Morgenroth 1999). The elastic operation of a joint requires a significant distance between the joint axis and the line of action of the ground reaction force (Farley et al. 1998). If more than one joint fulfils this condition, the loads must be shared between these joints. With respect of multi-segment legs, this evokes the kinematic redundancy problem; i.e., the same leg length can be realized by different joint configurations. This problem was first addressed in Bernstein's motor equivalence problem (Bernstein 1967). There is no generally accepted theory available which could explain the observed behaviour in biological limbs (for review see Gielen et al. 1995). The approaches found in the literature postulate different optimization criteria which result in corresponding movement patterns taking physiological, energetic, or metabolic aspects into account. Nevertheless, these constraints did not explain the unique motor pattern used by biological systems for an intended movement. It is well accepted that biological actuators are adapted to their mechanical environment and to different task-depending requirements (van Leeuwen 1992). By their intrinsic properties muscles may help to stabilize cyclic joint rotations in the case of sudden disturbances (Wagner and Blickhan 1999).

A key to solve the kinematic redundancy problem (Gielen et al. 1995) is the assumption of spring-like muscle behaviour (Winters 1995), as this defines a potential which specifies local minima at distinct joint

Correspondence to: A. Seyfarth
(Tel.: +49-3641-945720, Fax: +49-3641-945702
e-mail: oas@uni-jena.de)

configurations. However, the quasi-elastic muscle operation is not sufficient to guarantee stable joint configurations (Dornay et al. 1993). To investigate the interplay between elastically operating actuators, leg architecture, and motor program, a mechanical model is required. A simple model recently introduced by Farley et al. (1998) represented torque actuators as linear rotational springs at ankle, knee, and hip joints within a four-segment model. The observed torque characteristics, however, rather suggest nonlinear torque characteristics in the ankle and knee joints. Due to the small distance to the line of action of the ground reaction force, the hip joint did not show elastic behaviour. If elastic joint operation is assumed in such situations kinematic instabilities will appear. The stability was not addressed in their study.

The aim of our study is to explore the requirements of elastically operating torque actuators of a kinematically redundant segmented leg. Thereby the influence of the segment length design and different kinematic conditions are taken into account. At least three leg segments are necessary to address kinematic redundancy. The leg design will be judged by investigating the possible kinematic responses to different loading situations. The stability and predictability of the leg operation will be quantified by calculating the configurations of inherent leg instability. This allows the derivation of criteria for leg length design, motor control (torque adjustment), and kinematic programs. The effects of segment inertia are neglected, as they are of minor importance during fast types of locomotion.

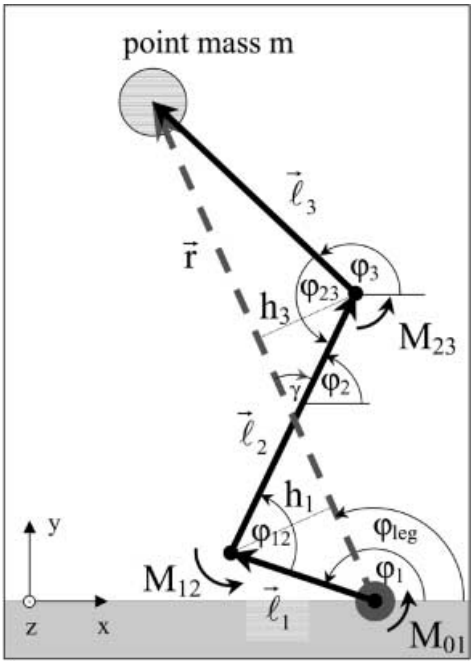

Fig. 1. Three-segment model with one point mass. Torques are applied at ball, ankle, and knee joints (M_{01}, M_{12} and M_{23}). The leg configuration is represented by the inner joint angles (ankle angle: $\varphi_{12} = \varphi_2 + \pi - \varphi_1$, knee angle: $\varphi_{23} = \varphi_2 + \pi - \varphi_3$). The angle γ is defined as the difference between middle segment and leg orientation: $\gamma = \varphi_2 - \varphi_{\text{leg}}$ (in this sketch γ is negative)

2 Methods

2.1 The three-segment model

The planar model (Fig. 1) consists of the following parts: (1) a point mass m representing the total body mass, and (2) three massless leg segments (foot, shank, and thigh; lengths l_1, l_2 and l_3), linked by frictionless rotational joints. The point mass is attached at the top of the thigh (hip). As there is only one point mass the equations of motion are:

$$m\ddot{\mathbf{r}} = \mathbf{F}_{\text{leg}} + m\mathbf{g} \ , \tag{1}$$

where $\mathbf{r}$ is the position of the point mass, $\mathbf{F}_{\text{leg}}$ is the force due to the operation of the leg segments, and $\mathbf{g}$ is the gravitational acceleration vector. As all segments are massless the force $\mathbf{F}_{\text{leg}}$ acting on the point mass is equal to the external ground reaction force.

2.2 Torque equilibrium

To integrate the equations of motion (1) the instantaneous leg force $\mathbf{F}_{\text{leg}}$ has to be calculated. In contrast to the dynamics of the point mass, we neglect all dynamic effects due to segment inertias within the leg. The position of the point mass with respect to the point of ground support determines the instantaneous leg length. This length is directly related to leg force if conservative (angle-dependent) torque actuators are present at the knee and ankle joints. In the case of external torques (e.g., at the ball of the foot) a further influence of the leg orientation with respect to the ground exists.

The torques at the hinge joints (ball M_{01}, ankle M_{12}, and knee M_{23}) and the orientation of the leg segments $(\mathbf{l}_1, \mathbf{l}_2, \mathbf{l}_3)$ must fulfil the following static torque equilibrium (all M_{ij} direct in z; for details see Appendices A–C):

$$\begin{aligned} (\mathbf{l}_1 \times \mathbf{F}_{\text{leg}})\big|_z &= M_{01} - M_{12} \\ (\mathbf{l}_2 \times \mathbf{F}_{\text{leg}})\big|_z &= M_{12} - M_{23} \\ (\mathbf{l}_3 \times \mathbf{F}_{\text{leg}})\big|_z &= M_{23} \end{aligned} \tag{2a–c}$$

where

$$\mathbf{l}_1 + \mathbf{l}_2 + \mathbf{l}_3 = \mathbf{r} \ . \tag{2d}$$

These are five algebraic equations to estimate the following five unknowns: the leg force $\mathbf{F}_{\text{leg}}$ (two components), and the segment angles φ_1, φ_2 and φ_3. Hereby constant segment lengths $|\mathbf{l}_i| = l_i$, a given leg vector $\mathbf{r}$, and given torques $M_{ij}(\varphi_1, \varphi_2, \varphi_3; t)$ were assumed.

The segment angles φ_1, φ_2, and φ_3 may be substituted by the leg angle φ_{leg} and by two variables representing the internal leg configuration (e.g., φ_{12}, φ_{23} or h_1, h_3; Fig. 1). As the leg length $r = |\mathbf{r}|$ merely depends on the internal leg configuration we separate $\mathbf{r} = r(\varphi_{12}, \varphi_{23}) \cdot \mathbf{e}_r(\varphi_{\text{leg}})$ where $\mathbf{e}_r$ represents the unit vector uniquely determined by the leg orientation $\varphi_{\text{leg}}(\mathbf{r})$ and

$$r(\varphi_{12},\varphi_{23}) = \sqrt{l_1^2 + l_2^2 + l_3^2 - 2l_1l_2\cos\varphi_{12} - 2l_2l_3\cos\varphi_{23} + 2l_1l_3\cos(\varphi_{12}-\varphi_{23})}\ . \tag{3}$$

After replacing (2d) by (3) four equations now exist for the following unknowns: two components of the leg force $\mathbf{F}_{\text{leg}}$ and two variables representing the internal leg configuration. The internal configuration is a consequence of the chosen torque characteristics at the joints and must fulfil (3). For torque characteristics only depending on the internal configuration $M_{ij}(\varphi_{12},\varphi_{23})$ we can identify all configurations of φ_{12}, and φ_{23} fulfilling the torque equilibrium (2a–c) denoted by $Q(\varphi_{12},\varphi_{23})=0$.

$$Q(\varphi_{12},\varphi_{23}) = \frac{M_{12}}{l_1}\sin\varphi_{23} + \frac{M_{12}-M_{23}}{l_2}\sin(\varphi_{12}-\varphi_{23}) + \frac{M_{23}}{l_3}\sin\varphi_{12} = 0 \tag{7}$$

The internal leg configuration characterized by (3) and (7) requires to know the torque characteristics (see below). The amount of leg force F_{leg} remains to be estimated using either (2a–c) or (4a,b) resulting in:

$$F_{\text{leg}}(\varphi_{12},\varphi_{23}) = \frac{r(\varphi_{12},\varphi_{23})\cdot\left(\frac{M_{12}}{l_1}\sin\varphi_{23} + \frac{M_{12}+M_{23}}{l_2}\sin(\varphi_{12}-\varphi_{23}) - \frac{M_{23}}{l_3}\sin\varphi_{12}\right)}{l_1(\cos\varphi_{23}-\cos(2\varphi_{12}-\varphi_{23})) + 2l_2\sin\varphi_{12}\sin\varphi_{23} + l_3(\cos\varphi_{12}-\cos(\varphi_{12}-2\varphi_{23})) - 2\frac{l_1l_3}{l_2}\sin^2(\varphi_{12}-\varphi_{23})} \tag{8}$$

In this paper these solutions of $Q(\varphi_{12},\varphi_{23})=0$ will be derived for simplified situations. After estimating the joint angles using $Q(\varphi_{12},\varphi_{23})=0$ and (3), the leg force is simply given by two linearly independent equations (2a–c).

2.3 Neglecting the external torque M_{01}

To find a first solution of the torque equilibrium, the torque at the ball of the foot is neglected: $M_{01}=0$. This results in leg forces $\mathbf{F}_{\text{leg}}$ always parallel to $\mathbf{r}$ as we can summarise (2a–c) to $\mathbf{r}\times\mathbf{F}_{\text{leg}}\big|_z = M_{01}$. For joint torques M_{12} and M_{23} only depending on the internal configuration ($\varphi_{12},\varphi_{23}$; Fig. 1), the amount of the leg force also does not depend on the leg orientation φ_{leg}. As (2b) becomes the negative sum of (2a) and (2c), only two remaining torque equations must be fulfilled:

$$h_1\cdot F_{\text{leg}} = M_{12},\quad -h_3\cdot F_{\text{leg}} = M_{23}\ , \tag{4a,b}$$

or eliminating F_{leg}:

$$Q(\varphi_{12},\varphi_{23}) = M_{12}h_3 + M_{23}h_1 = 0\ , \tag{5}$$

where $h_1(\varphi_{12},\varphi_{23})$ and $h_3(\varphi_{12},\varphi_{23})$ are the distances of the joints to the line of action of the leg force $h_i = l_i\sin(\mathbf{l}_i,\mathbf{r})$:

$$\boldsymbol{\nabla}_{\boldsymbol{\varphi}} r(\varphi_{12},\varphi_{23}) = \begin{pmatrix} \frac{\partial r(\varphi_{12},\varphi_{23})}{\partial\varphi_{12}} \\ \frac{\partial r(\varphi_{12},\varphi_{23})}{\partial\varphi_{23}} \end{pmatrix} = \begin{pmatrix} h_1 \\ h_3 \end{pmatrix} \tag{6}$$

that is, $h_1>0$ and $h_3>0$ in Fig. 1. Equation (5) determines the ratio of ankle to knee torque M_{12}/M_{23} to be equal to $-h_1/h_3$ as long as the foot contacts the ground at the ball with no external torque ($M_{01}=0$; no effects of heel or toe contact). In terms of the inner joint angles, the simplified torque equilibrium (5) results in the requested Q function:

where $r(\varphi_{12},\varphi_{23})$ denotes the instantaneous leg length (3).

2.4 Potential energy and leg length at $Q=0$

In the case of conservative torque actuators at the knee and ankle joints the torque equilibrium (5, 7) is equivalently represented by a dependency between the potential energy $E(\varphi_{12},\varphi_{23})$ and the leg length $r(\varphi_{12},\varphi_{23})$:

$$\boldsymbol{\nabla}_{\boldsymbol{\varphi}} E(\varphi_{12},\varphi_{23}) = \beta(\varphi_{12},\varphi_{23})\cdot\boldsymbol{\nabla}_{\boldsymbol{\varphi}} r(\varphi_{12},\varphi_{23})\ , \tag{9}$$

where

$$\beta(\varphi_{12},\varphi_{23}) = \frac{\boldsymbol{\nabla}_{\boldsymbol{\varphi}} E\cdot\boldsymbol{\nabla}_{\boldsymbol{\varphi}} r}{\left|\boldsymbol{\nabla}_{\boldsymbol{\varphi}} r\right|^2} = -F_{\text{leg}}(\varphi_{12},\varphi_{23}) \tag{10}$$

is the negative leg force F_{leg} and

$$\boldsymbol{\nabla}_{\boldsymbol{\varphi}} E(\varphi_{12},\varphi_{23}) = \begin{pmatrix} -M_{12} \\ M_{23} \end{pmatrix} \tag{11}$$

in the case of monoarticular torque characteristics $M_{12}(\varphi_{12})$ and $M_{23}(\varphi_{23})$. Equation (9) is a sufficient condition for a local extreme of $E(\varphi_{12},\varphi_{23})$ on a $r(\varphi_{12},\varphi_{23}) = const.$ line. The equivalence of (9) with $Q=0$ becomes obvious by multiplying $\boldsymbol{\nabla}_{\boldsymbol{\varphi}} E(\varphi_{12},\varphi_{23})$ with any vector $\mathbf{t}_r(\varphi_{12},\varphi_{23})$ perpendicular to $\boldsymbol{\nabla}_{\boldsymbol{\varphi}} r(\varphi_{12},\varphi_{23})$ (6). The stability of a configuration fulfilling the torque equilibrium (or Eq. 9, respectively) requires an increase of E for displacements in the internal joint configuration $(\varphi_{12},\varphi_{23})$ along $r=const.$ nearby the solution of $Q=0$. The corresponding conditions are derived in the Appendix D.

2.5 Symmetrical loading: stiffness equilibrium

To investigate the influence of knee and ankle rotational stiffness, linear ($v=1$) or, more generally, nonlinear ($v>0$, $v\neq 1$) rotational springs are introduced:

$$M_{12} = c_{12}(\varphi_{12}^0 - \varphi_{12})^v \ , \tag{12a}$$

$$M_{23} = -c_{23}(\varphi_{23}^0 - \varphi_{23})^v \ , \tag{12b}$$

where φ_{12}^0 and φ_{23}^0 are the nominal angles of the rotational springs, φ_{12} and φ_{23} are the joint angles (with $\varphi_{ij} < \varphi_{ij}^0$), c_{12} and c_{23} are the rotational stiffnesses, and v is the exponent of nonlinearity. Such a joint torque characteristic is present in humans and several mammals during fast locomotion (Stefanyshyn and Nigg 1998). The nonlinearity may result from tendon properties and muscle-tendon dynamics.

For the particular case of symmetrical loading with $\varphi_{12}^0 = \varphi_{23}^0$ and $\varphi_{12} = \varphi_{23}$, the torque equilibrium (5) results in

$$\frac{c_{12}(\varphi_{12}^0 - \varphi_{12})^v}{l_1 \sin(\varphi_{12} - \gamma)} = \frac{c_{23}(\varphi_{23}^0 - \varphi_{23})^v}{l_3 \sin(\varphi_{23} - \gamma)} \tag{13}$$

which requires:

$$\frac{c_{12}}{l_1} = \frac{c_{23}}{l_3} \ , \tag{14}$$

where $\gamma(\varphi_{12}, \varphi_{23})$ is the intersectional angle between $\mathbf{l}_2$ and $\mathbf{r}$ (see Fig. 1). Thus, if the ratio of ankle to knee stiffness is equal to the ratio of the foot to thigh segment length, a symmetrical loading of the system is a solution of the torque equilibrium (5, 7). *The stiffness equilibrium (14) does not depend on* l_2.

2.6 Introduction of normalized segment lengths and the stiffness ratio

As there is no influence of the total leg length, $l_{MAX} = l_1 + l_2 + l_3$, on either the torque equilibrium (5, 7) or on the stiffness equilibrium (14), we can substitute the actual segment lengths by a normalized length $\lambda_i = l_i / l_{MAX}$. To fulfil a symmetrical shortening, only the ratio of the rotational stiffnesses $R_C = c_{12}/c_{23}$ is crucial. The stiffness equilibrium (14) requires the ratio R_C to be equal to the length ratio $R_\lambda = \lambda_1/\lambda_3$, or:

$$R_C / R_\lambda = 1 \ . \tag{15}$$

2.7 Transition between zigzag and bow mode ($h_1 = 0$ or $h_3 = 0$, respectively)

Two qualitatively different geometrical configurations of the segmental arrangement can be distinguished. In Fig. 1 the leg joints (ankle and knee) are arranged in a 'zigzag' mode. Here both joints are located at opposite sides with respect to the leg axis. However, there is another possible geometrical arrangement for the same leg length: the 'bow' mode where knee and ankle joint lie on the same side.

The actual configuration of the leg depends not merely on the leg length but is largely determined by the torque characteristics at the leg joints. Nevertheless, multiple solutions of possible leg configurations might be present for given torque characteristics (e.g., like Eqs. 12a,b; see Sect. 3). A transition between the zigzag and bow modes requires particular geometrical conditions: angle configurations where either the ankle ($h_1 = 0$) or the knee ($h_3 = 0$) joint is crossing the leg axis. These configurations can be expressed as follows (Fig. 2A,B): $h_1 = 0$ is fulfilled for

$$\tan\varphi_{12} = \frac{\sin\varphi_{23}}{\cos\varphi_{23} - \lambda_2/\lambda_3} \tag{16a}$$

and $\varphi_{12} = \varphi_{12}^0$ (in the case of monoarticular actuators); or $h_3 = 0$ is fulfilled for

$$\tan\varphi_{23} = \frac{\sin\varphi_{12}}{\cos\varphi_{12} - \lambda_2/\lambda_1} \tag{16b}$$

and $\varphi_{23} = \varphi_{23}^0$ (in the case of monoarticular actuators).

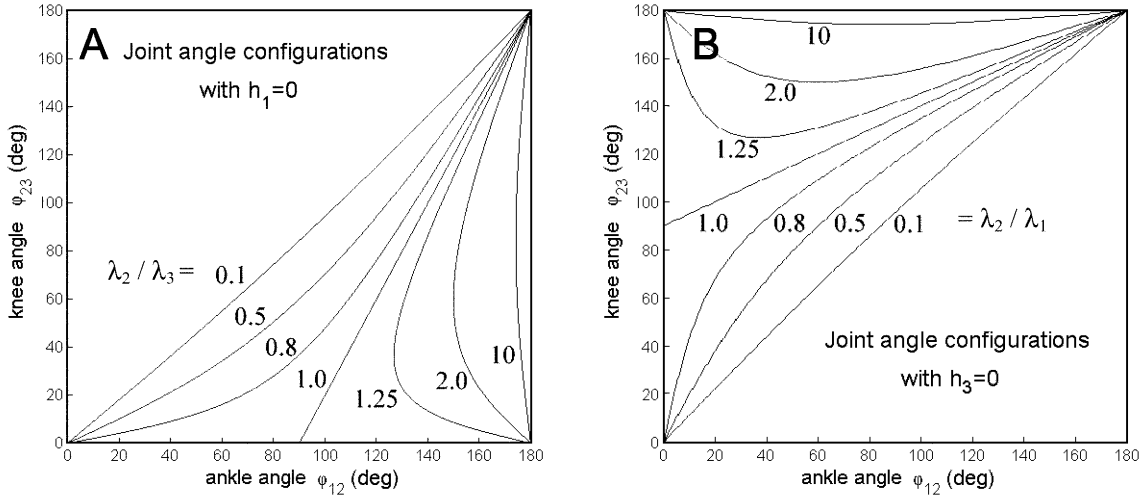

Fig. 2A,B. Joint angle configurations where (**A**) the ankle joint ($h_1 = 0$) and (**B**) the knee joint ($h_3 = 0$) coincides with the leg axis for different segment length designs (denoted by λ_2/λ_3 and λ_2/λ_1; Eq. 16a,b)

2.8 Numerical investigation of the model

Two different approaches were applied to investigate the three-segment model: (i) *forward dynamic modelling* of the equations of motion (1), and (ii) mapping the *solutions of the torque equilibrium* (5, 7). In this article the results of the second approach are presented in terms of the possible leg configurations $(\varphi_{12}, \varphi_{23})$ with respect to: (a) the nominal angle configuration $(\varphi_{12}^0, \varphi_{23}^0)$, (b) the segment length design (λ_2, $R_\lambda = \lambda_1/\lambda_3$), and (c) the torque design (stiffness ratio R_C, exponent v). The influence of nonconservative structures (e.g., heel strike, represented by $M_{01}(\varphi_1, \dot{\varphi}_1)$), segment inertias, and continuous changes of the nominal angles on the joint kinematics may be investigated applying the first approach, and will be discussed.

3 Results

We aim to identify the construction and control strategies of the three-segment leg for a well-behaving (i.e., homogeneous and stable) loading of the elastic joints. We approach this issue by exploring the behaviour of the static solutions of the torque equilibrium (5, 7) for some representative examples of leg design (Fig. 3). Starting with solutions fulfilling the stiffness equilibrium resulting in symmetrical joint flexions we

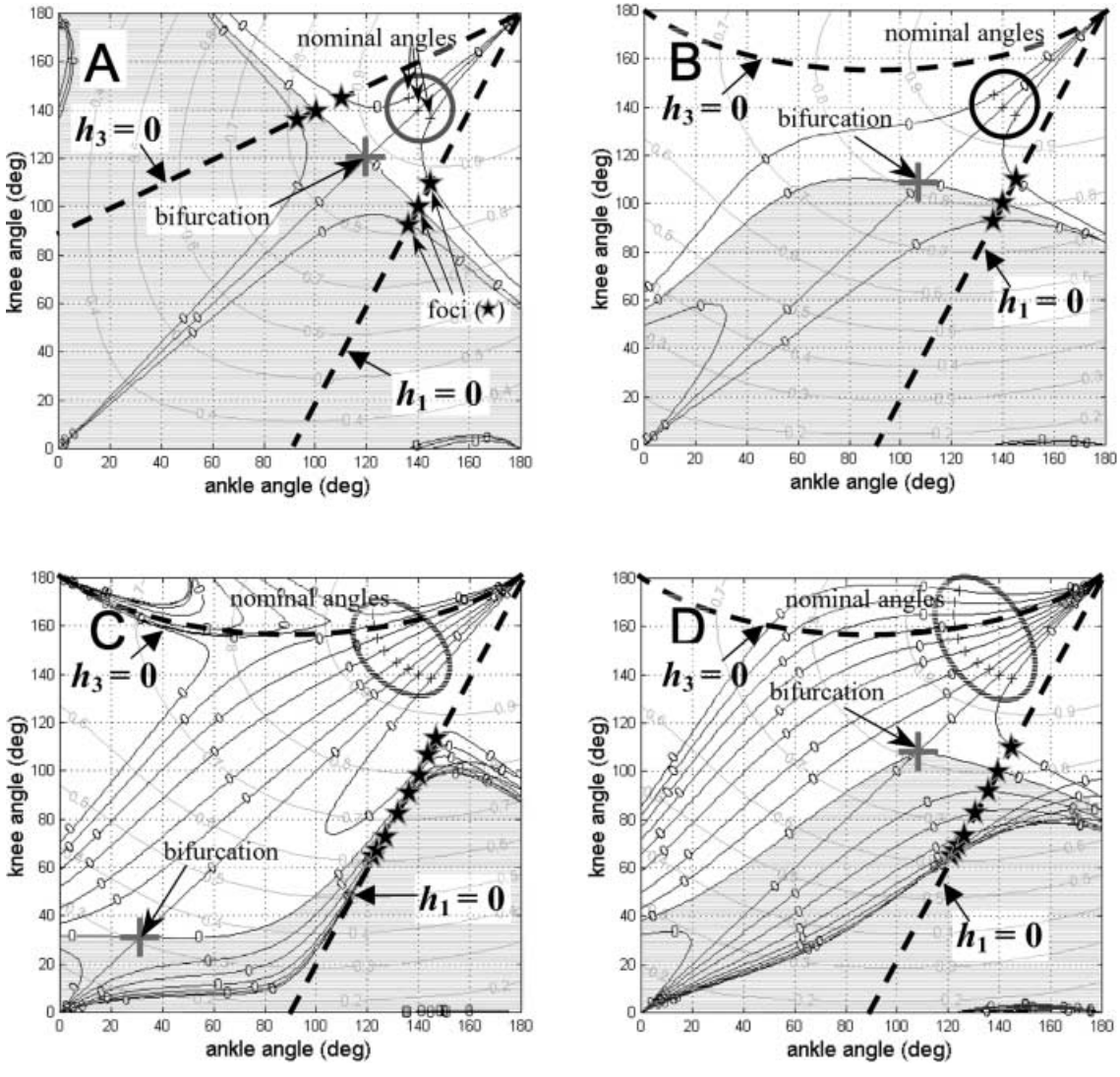

Fig. 3A–D. Solutions of the torque equilibrium (Eq. 5; $Q = 0$ denoted by *lines with circles*) in the configuration space (φ_{12}, φ_{23}) with different leg designs and torque characteristics (see below) fulfilling the stiffness equilibrium (Eqs. 14, 15: $R_C = R_\lambda$) and nominal angles at a relative nominal leg length $\lambda_0 = 0.94$. The *grey areas* represent restrictions due to the oblique solution. Configurations with a constant relative leg length $\lambda(\varphi_{12}, \varphi_{23}) = const.$ are denoted by *grey lines* with embedded length values (0.2–0.9). Configurations where joints are crossing the leg axis ($h_1 = 0$ or $h_3 = 0$) are denoted schematically by bold dashed lines. Leg designs: (**A**) equal segment lengths 1:1:1 (all $\lambda_i = 1/3$, i.e., $R_\lambda = 1$), (**B**, **C**, **D**) human-like leg design $\lambda_1{:}\lambda_2{:}\lambda_3 = 2{:}5{:}5$ ($R_\lambda = 2/5$). Torque characteristics: (**A**, **B**) linear rotational springs at ankle and knee joint, (**C**) quadratic characteristic ($v = 2$; $M_{ij} \sim \Delta\varphi_{ij}^2$), (**D**) linear rotational springs plus a biarticular spring ($M_{13} = c_{13}\Delta\varphi_{13}$ with $\Delta\varphi_{13} = \varphi_{23} - \varphi_{12}$, $c_{13} = 0.05\, c_{23}$)

complete our consideration by giving some examples with asymmetric joint configurations.

3.1 General description

For a leg with *conservative torque characteristics* at the ankle and knee joints (e.g., rotational stiffnesses; Eq. 12) we can consider all possible joint configurations within the configuration space $(\varphi_{12}, \varphi_{23})$ (Fig. 3). Hereby the influence of the leg orientation with respect to the ground on the leg force (e.g., due to an external torque like M_{01}) is neglected.

A symmetrical operation of both joints $(\varphi_{12} = \varphi_{23})$ requires a stiffness adjustment according to the outer segment lengths (stiffness equilibrium; Eq. 14). This fulfils *zigzag mode* with an opposite arrangement of ankle and knee with respect to the leg axis (Fig. 1). Errors in the stiffness ratio or nominal angle adjustment deflect the solutions from the symmetrical solution and may lead to an extension of one joint while leg shortening. Consequently, a transition into the *bow mode* may occur where both joints are at the same side with respect to the leg axis (Fig. 3A).

The three segment leg tends to leave the symmetrical joint configuration. Even an optimal joint stiffness adjustment (14) can not guarantee the parallel operation of both joints. Depending on the nominal configuration of the leg φ_0 (i.e., the joint angles for zero leg force) there exist odd solutions of the torque equilibrium intersecting the symmetrical axis at distinct leg lengths (Fig. 3). This results in up to three paths being possible for further leg shortening (Fig. 3A,B). The symmetrical branch with $\varphi_{12} = \varphi_{23}$ proves to be unstable (Appendix D). As two branches remain to be considered we call this intersection a *bifurcation* (Fig. 3A).

For the case of *symmetrical loading* (equal nominal angles and stiffness equilibrium), the dependency between

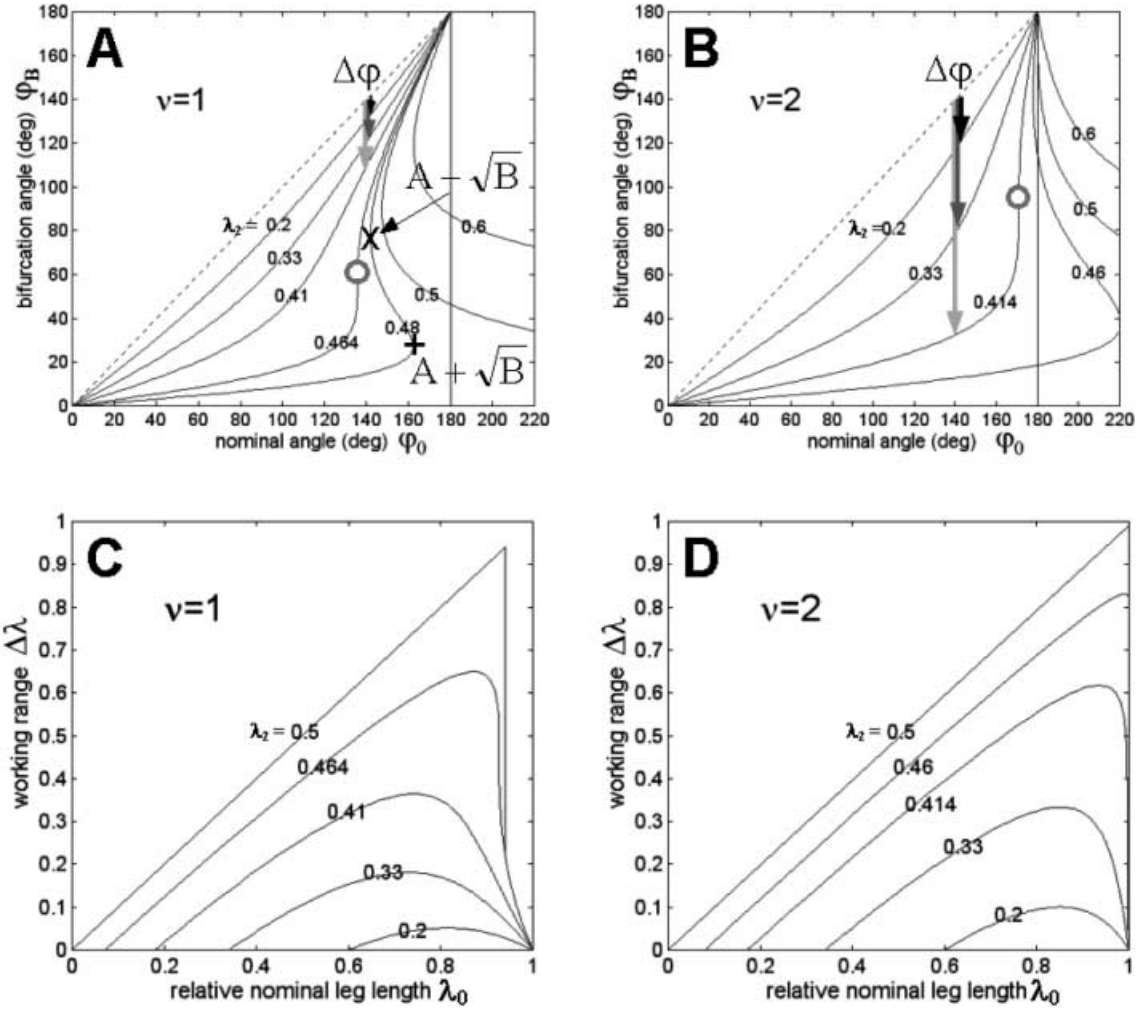

Fig. 4A–D. Bifurcations in symmetrical loading: **A**, **B** for each nominal angle φ_0 and a given exponent ν of the torque characteristic, the location of the possible bifurcation angle(s) φ_B depend merely on λ_2 and not on R_λ. If λ_2 exceeds a critical threshold $\lambda_{2,I\to II}(\nu)$ (*small circles*) a sudden change in φ_B occurs at a corresponding nominal angle $\varphi_{0,Crit}(\lambda_2, \nu)$. Then, new bifurcations appear for $\varphi_0 > \varphi_{0,Crit}$ which reduce the working range $\Delta\varphi$ (*small arrows*). The local extremes in $\varphi_0(\varphi_B)$ (E4) determine the existence of type I (*symbol* '+': $\cos\varphi_{B,Extr} = A + \sqrt{B}$) or type II (*symbol* '×': $\cos\varphi_{B,Extr} = A - \sqrt{B}$; Eq. E5) bifurcations; **C**, **D** relative working range $\Delta\lambda = \lambda_0(\varphi_0) - \lambda_B(\varphi_B)$ for different λ_2-designs depending on the relative nominal leg length λ_0 and ν (but not on R_λ). The highest advantage of nonlinear (quadratic) torque design is found for $\lambda_2 = 0.3$–0.5 and $\lambda_0 > 0.8$

the bifurcation angle φ_B and the nominal angle φ_0 can be expressed in one algebraic equation $\varphi_0(\varphi_B)$ (see Eq. E3). There are only two parameters influencing the shape of the $\varphi_0(\varphi_B)$ function (Fig. 4A,B; summarized in Fig. 8): the relative length of the middle segment λ_2 and the exponent v of the torque characteristic. The difference between the nominal angle and the bifurcation angle (or the corresponding leg lengths) is a measure of stable leg shortening which we denote as the angular *working range* $\Delta\varphi$ (or as the translational working range $\Delta\lambda$, respectively).

Two types of bifurcations can be distinguished. The *type I* bifurcation limits the working range for *all* nominal angles φ_0 if $\lambda_2 < 1/2$. While increasing φ_0, a *sudden decrease in working range* may occur at a critical nominal angle $\varphi_{0,Crit}$ due to an inserted *type II* bifurcation (see Fig. 8). Even both bifurcations may occur in a very small region in λ_2 and v, which results in *up to three intersections* of odd solutions with the symmetrical axis (e.g., $\lambda_2 = 0.48$ in Fig. 4A). This region is very important for legs with relative middle segment lengths $\lambda_2 < 1/2$, as here the maximum working range is obtained.

Different optimal nominal configurations φ_0 (which corresponds to λ_0 in Fig. 4C,D) exist for either maximum angular *or* maximum translational working range at a given middle segment length λ_2 and an exponent v of the torque characteristic (Fig. 5). For exponents $v < 3$ the type II bifurcation threatens to reduce the symmetrical working range if the relative middle segment length approaches 1/2 (thin black lines in Fig. 5, compare to Fig. 4C). The region in λ_2 and v with an effective reduction in the translational working range $\Delta\lambda$ due to a type II bifurcation (black area in Fig. 5B,D) is smaller than the corresponding reduction in the angular working range $\Delta\varphi$ (black area in Fig. 5A,C).

3.2 Specific statements and explanations

1. It is always possible to operate the three-segment leg with symmetrical joint configurations until a bifurcation. But it is not possible to continue the symmetrical path during shortening beyond the bifurcation. The mechan-

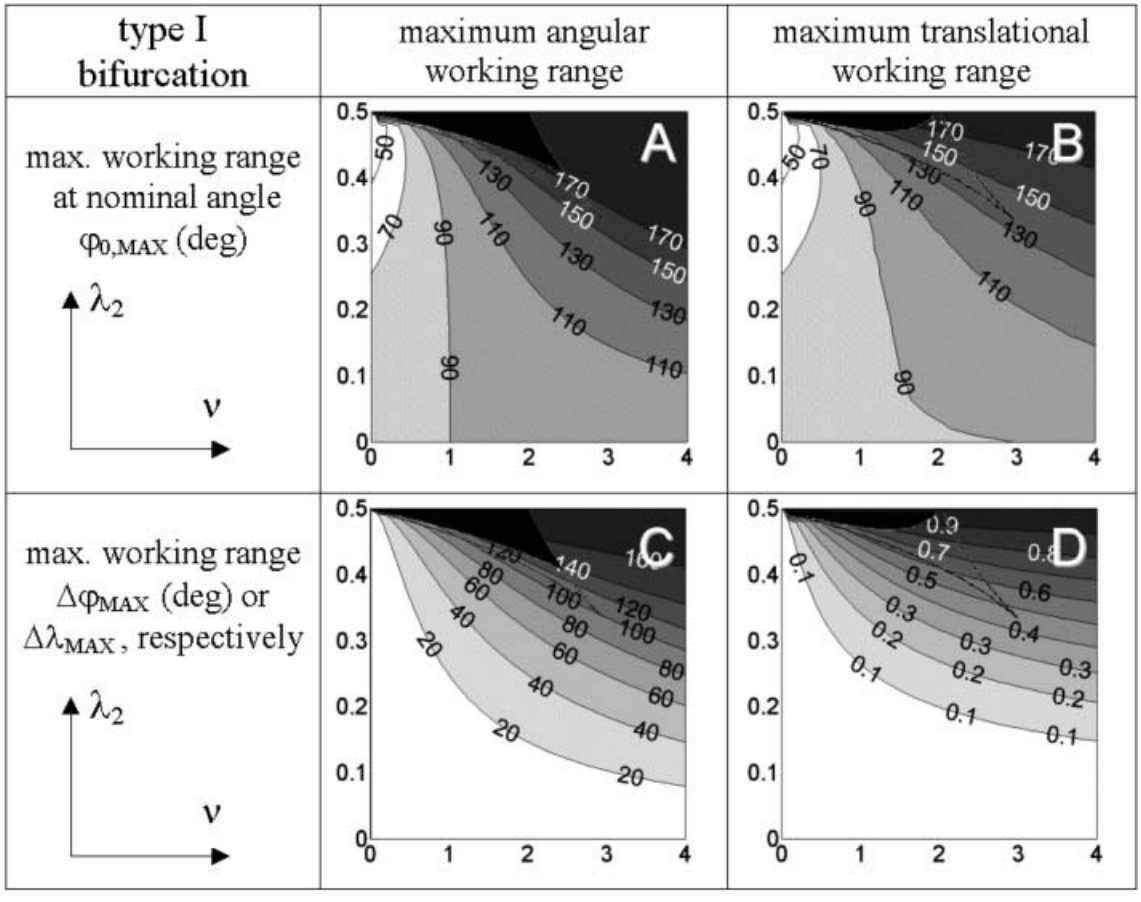

Fig. 5A–D. Symmetrical loading. Different nominal angle configurations φ_0 (**A**, **B**) are necessary to reach the maximum angular (**C**) or translational (**D**) working range for given leg designs λ_2 and torque characteristics v. For $\lambda_2 < 1/2$ a type I bifurcation always restricts the working range (Fig. 9). In the area surrounded by the *thin line*, a type II bifurcation may further reduce (Fig. 11A,B) the working range if the critical nominal angle $\varphi_{0,Crit}$ (Fig. 8) is exceeded (denoted by the *black area*). With increasing v the nominal angle $\varphi_{0,MAX}$ (**A**, **B**) and the corresponding maximum working ranges $\Delta\varphi_{MAX}$ (**C**) or $\Delta\lambda_{MAX}$ (**D**) are shifted to higher values. Also, an increase in λ_2 leads to higher maximum working ranges (**C**, **D**) and for about $v > 1$ to higher $\varphi_{0,MAX}$ (**A**, **B**) as well. For maximum translational working range (**D**), slightly lower nominal angles (**B**) are necessary than for maximum angular working range (**A**, **C**). For $\lambda_2 > \lambda_{2,I\to II}$, a type II bifurcation is inserted if $\varphi_{0,MAX} > \varphi_{0,Crit}$ is fulfilled (*black area*). Due to the more flexed leg operation optimizing the translational rather than the angular working range the disturbance by the type II bifurcation is reduced to a smaller area within the (λ_2, v)-space

ical stability of the system with respect to perturbations at a given leg length r changes from stable to unstable if a bifurcation occurs (Appendix D). Therefore, the translational (rotational) working range in the zigzag mode is only guaranteed between the nominal length (angle) and the bifurcation length (angle). Nearby the nominal configuration the system is always stable due to the local minimum of the potential energy E at this point. This is a consequence of the fact that the curvature of the scalar field E is exceeding any limit while the curvature of r remains limited whilst approaching the nominal configuration (Eq. D4). The limitation due to the bifurcation even holds for solutions with changed nominal configurations $\varphi_{12}^0 \neq \varphi_{23}^0$ at a given nominal length λ_0 and $R_C = R_\lambda$: the odd branch can not be crossed by these solutions (Fig. 3A).

2. Both remaining odd branches are accessible if they allow further leg shortening. In the case of equal outer segment lengths ($R_\lambda = 1$) and symmetrical loading ($\varphi_{12}^0 = \varphi_{23}^0$ and $R_C = R_\lambda$) both branches are stable (Fig. 3A). However, in most cases the odd branch is crossing the $r = const.$ line at the bifurcation point (Fig. 6). Then the only branch which allows further leg shortening is stable and will be chosen (for stability conditions see Appendix D). Even without a bifurcation a sudden change in stability may occur if further leg shortening is prohibited due to the alignment of the solution of the torque equilibrium $Q = 0$ with a $r = const.$ line. Such a situation is illustrated in Fig. 6 and occurs in solutions adjacent to the symmetrical solution in the case of unequal outer segment lengths (in Fig. 3C, between the $h_1 = 0$ line and the symmetrical axis). Further leg shortening can not be achieved within the static torque equilibrium. A leg with inertias or friction would swap into an adjacent torque equilibrium at this leg length.

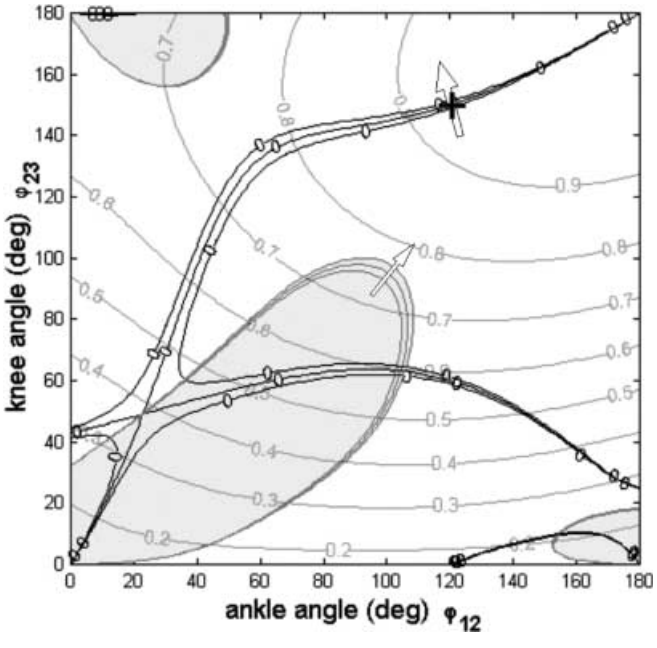

Fig. 6. Stability analysis of solutions for $Q = 0$ (Eq. 5; *lines with circles*) in the configuration space $(\varphi_{12}, \varphi_{23})$ for a human leg design 2:5:5 and slightly varied nominal configuration $\varphi_{12}^0 = 120 \pm 0.5°$, $\varphi_{23}^0 = 150 \pm 1°$ (denoted by '+'), $R_C = 0.596$, $v = 1$. The system is unstable in the grey areas ($\Delta E < 0$ in Eq. D4). The transition between stable and unstable behaviour occurs either at a bifurcation ($\mathbf{\nabla} Q = 0$, near to left lower corner) or if the $Q = 0$ line aligns with an $r = const.$ line ($\mathbf{t}_r^T \mathbf{\nabla} Q = 0$; e.g., at about $\varphi_{12} = 100°$, $\varphi_{23} = 60°$). The *grey* $r = const.$ *lines* denote the leg lengths (0.2–0.9). The area of instability slightly depends on the nominal angles. The arrows denote the tendency with respect to the varied nominal configuration

3. A transition from the zigzag into the bow mode requires a focus at a $h = 0$ line. The limit between bow and zigzag mode is given by the $h_1 = 0$ and $h_3 = 0$ lines (see Sect. 2, Fig. 2). In the case of monoarticular actuators (12a,b), one joint (ankle or knee, respectively) must be in its nominal position while crossing the leg axis (Table 1, Fig. 3A–C). The intersection of a $Q = 0$ line with a $h = 0$ line occurs at the corresponding nominal angle regardless of the stiffness ratio R_C, the remaining nominal angle and the exponent v of the torque characteristic. As this particular configuration is very attractive to solutions of the torque equilibrium we denote it as a focus (Fig. 3). The geometry of the $h = 0$ lines is determined by the segment length design (Eq. 16; Figs. 3 and 7B).

4. When bypassing the bifurcation the working range can be extended. If one outer segment λ_1 (or λ_3) is smaller than λ_2 there is no focus in one half of the configuration space $\varphi_{12} < \varphi_{23}$ (or $\varphi_{12} > \varphi_{23}$, respectively) if the corresponding nominal angle φ_{23}^0 (or φ_{12}^0, respectively) is smaller than the critical joint angle $\varphi_{23,\mathrm{Crit}}$ (or $\varphi_{12,\mathrm{Crit}}$, respectively; Table 1). Furthermore, in the case of unequal outer segment lengths $R_\lambda \neq 1$ (Fig. 7D) the odd branch crossing the bifurcation is deflected (Fig. 3B). This facilitates almost homogeneous bending which continues shortening on the stable odd branch that remains in the zigzag mode. In this case, nominal angle configurations shifted into the well-behaving half-space $\varphi_{12} < \varphi_{23}$ (or $\varphi_{12} > \varphi_{23}$, respectively) are suited for a high working range without crossing a bifurcation (Fig. 3B).

5. The symmetrical working range depends on the relative length of the middle segment but not on the ratio of the outer segment lengths. In Appendix E an analytical function is derived describing the dependency between the nominal angle φ_0 and the bifurcation angle φ_B in the case of symmetrical loading $\varphi = \varphi_{12} = \varphi_{23}$ (E3), which

Table 1. The minimum of the $h_3 = 0$ line (16b) expressed as $\varphi_{23}(\varphi_{12})$ is present for a critical knee angle $\varphi_{23,\mathrm{crit}}$ with a corresponding reference angle $\varphi_{12,\mathrm{Ref}}$. Solutions may be attracted by a focus at $h_3 = 0$ if nominal angles φ_{23} are larger than $\varphi_{23,\mathrm{crit}}$ (Fig. 2B, Fig. 3A)

λ_2 / λ_1	$\varphi_{23,\mathrm{Crit}}$	$\varphi_{12,\mathrm{Ref}}$
1.0	90°	0°
1.25	126.9°	36.9°
1.5	138.2°	48.1°
2.0	150.0°	58.8°
2.5	156.4°	65.1°
3.0	160.5°	70.1°
10	174.3°	81.2°

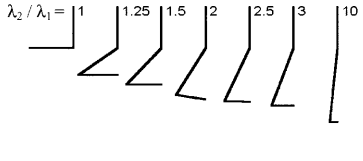

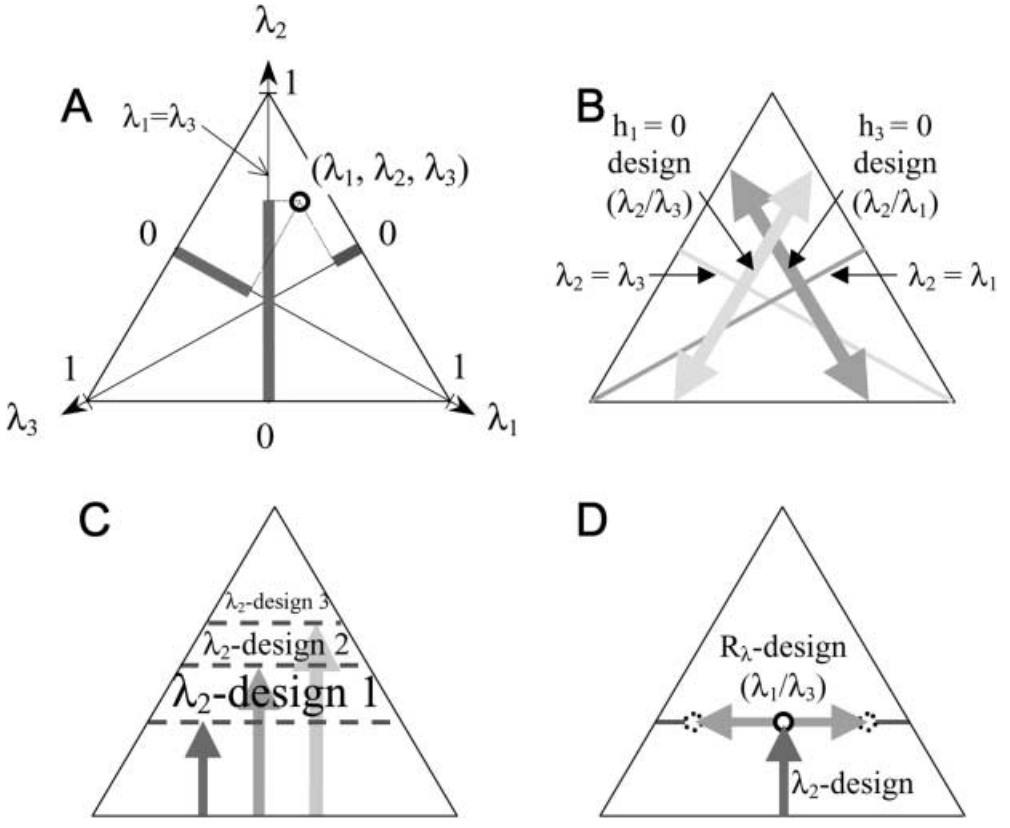

Fig. 7A. Segment length design is characterized by a triplet (λ_1, λ_2, λ_3) with $\lambda_1 + \lambda_2 + \lambda_3 = 1$; i.e. a point within the triangle. Different strategies of leg design can be distinguished: **B** To avoid the attraction of solutions by foci, the nominal angle design is restricted by the location of the $h = 0$ line (Figs. 2, 3; Table 1) in the chosen half of the configuration space (above or below the symmetrical axis $\varphi_{12} = \varphi_{23}$). **C** λ_2 is locating the bifurcation point(s) in symmetrical loading. **D** The R_λ design (ratio λ_1/λ_3) allows the advantage of asymmetric nominal configurations by properly adjusting the joint stiffness ratio R_C

is illustrated in Fig. 4A for an exponent $v = 1$. Two phenomena are striking in this $\varphi_B(\varphi_0)$ dependency: (i) the angular working range is largely influenced by the nominal angle φ_0, and (ii) exceeding a critical middle segment length $\lambda_{2,I\to II}$ there is a sudden change in the location of the bifurcation φ_B which limits the symmetrical working range $\Delta\varphi$, or $\Delta\lambda$ respectively (Fig. 4A,C: $v = 1$, $\lambda_{2,I\to II}(v) = 0.464$).

6. With increasing nominal angles, a sudden loss in symmetrical working range may occur. An inserted type II bifurcation (Appendix F) requires a nominal angle φ_0 which exceeds a critical angle $\varphi_{0,Crit}$ (Fig. 8B) and may occur even for $\lambda_2 > 1/2$ (Fig. 4A,B and Fig. 9). Within the configuration space an additional $Q = 0$ solution may be inserted with two intersections with the symmetrical solution. We denote the critical λ_2 at which the transition between type I and type II bifurcation may occur first time while increasing the relative middle segment length as $\lambda_{2,I\to II}$ (Fig. 10; Table 2). The loss in angular (translational) working range at this particular condition is illustrated in Fig. 11. The maximum critical angular (translational) working range occurs at $v = 1.5$ (or 0.8, respectively) and amounts to $\Delta\varphi_{Crit} \approx 85°$ ($\Delta\lambda_{Crit} \approx 0.47$).

7. The symmetrical working range is largely increased by a nonlinear torque characteristic. The angular working range (Fig. 3B,C) as well as the critical $\lambda_{2,I\to II}$ (Fig. 4-A,B; Fig. 10) is depending on the exponent v of the torque characteristic. The corresponding critical nominal angle $\varphi_{0,Crit}$ for the emergence of a type II bifurcation is illustrated in Fig. 8B. For a given nominal angle φ_0 between 140° and 160° the working range is significantly increased for an exponent $v = 2$ (Fig. 4B,D) as compared to $v = 1$ (Fig. 4A,C). Exponents between 1.5 and 2 result in an almost linear leg stiffness (not shown here). With high exponents ($v > 1.5$) the type II bifurcation may occur for smaller middle segment lengths (Fig. 4A,B; Fig. 10). However, the high critical nominal angles $\varphi_{0,Crit}$ of 160° or higher (Fig. 8B) prevent the type II bifurcation from reducing the working range.

8. In symmetrical loading of legs with a middle segment smaller than both outer segments the type II bifurcation is less relevant for optimal translational working range as compared to optimal angular working range (Fig. 5). For a maximum angular (Fig. 5C) or translational (Fig. 5D) working range a corresponding nominal angle (Fig. 5A,B) is required. At $\lambda_{2,I\to II}$ this nominal angle is still lower than the critical angle $\varphi_{0,Crit}$ for the insertion of the type II bifurcation. An effective reduction of the working range in symmetrical loading occurs only in the black areas in Fig. 5. Here the nominal angle for optimum working range exceeds $\varphi_{0,Crit}$ (Fig. 8B).

9. A small biarticular elastic structure may significantly increase the working range. In Fig. 3D a linear elastic biarticular actuator is introduced which operates similar to the human gastrocnemius muslce (knee flexor and ankle extensor), and has a nominal position at $\varphi^0_{13} = 0$ with $\varphi_{13} = \varphi_{23} - \varphi_{12}$ and $c_{13} = 0.05/c_{23}$. The working range in symmetrical loading is not influenced by the biarticular element. However, there is a strong influence in the upper half-space $\varphi_{12} < \varphi_{23}$ which results in largely

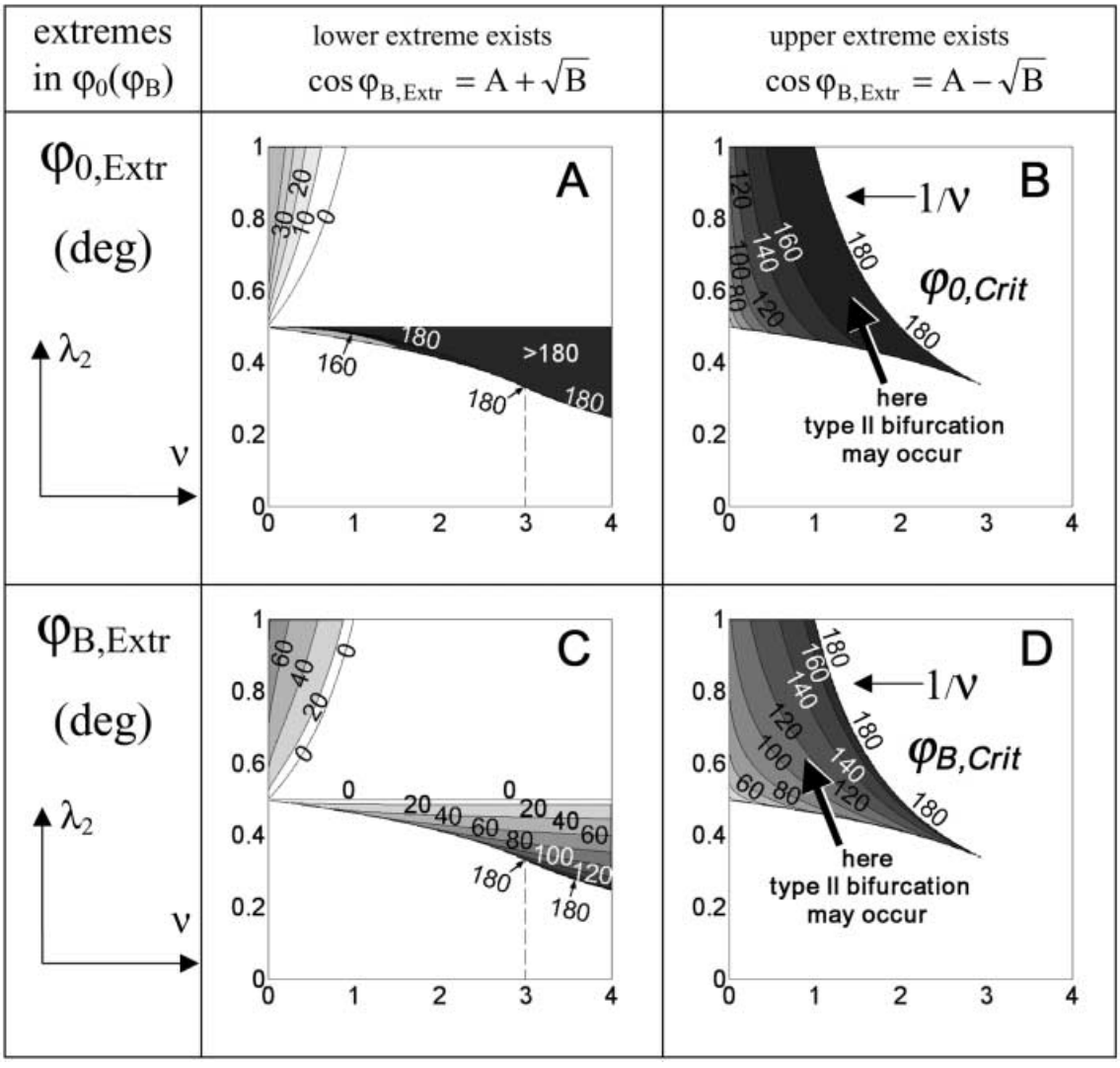

Fig. 8A–D. Regions in (λ_2, ν)-space where according to (E4) extremes in the $\varphi_0(\varphi_B)$ function occur with corresponding nominal $(\mathbf{A}, \mathbf{B})$ and bifurcation $(\mathbf{C}, \mathbf{D})$ angles. Solutions of $\cos\varphi_{B,Extr} = A + \sqrt{B}$ $(\mathbf{A}, \mathbf{C})$ and $\cos\varphi_{B,Extr} = A - \sqrt{B}$ $(\mathbf{B}, \mathbf{D})$ must be within $[-1, 1]$. Only the existence of the upper extreme (compare Fig. 4A,B) may lead to a sudden decrease in working range if φ_0 exceeds the $\varphi_{0,Crit}$ values shown in $(\mathbf{B})$ with a corresponding $\varphi_{B,Crit}$ shown in $(\mathbf{D})$. For $\lambda_2 > 1/\nu$, no type II bifurcation exists. The $\lambda_2 = 1/\nu$ line $(\mathbf{B}, \mathbf{D})$ corresponds to $\cos\varphi_B = -1$. In the case of pulling leg forces, a sudden decrease in working range occurs in leg lengthening $(\varphi > \varphi_0)$ for all $\varphi_0 \le \varphi_{0,Extr}$ $(\mathbf{A})$ and $\varphi_B \le \varphi_{B,Extr}$ $(\mathbf{C})$. This holds for $\lambda_2 > 1/(2-\nu)$ (upper left corner in Fig. 9), which is not relevant for human legs

parallel solutions for $Q = 0$ and a deflection of the odd branch to the symmetrical axis. The parallel alignment continues even into the bow mode (Fig. 3D) which allows elastic leg operation with almost-stretched knee angles.

10. There are also bifurcations for asymmetric nominal configurations $(\varphi_{12}^0 \neq \varphi_{23}^0)$. Leaving the symmetrical axis we can calculate a modified $R_C \neq R_\lambda$ (Appendix E) for getting again a solution directing to a bifurcation (Fig. 6). Similar to the symmetrical situation we can use this bifurcation to estimate a minimum guaranteed working range (Fig. 12) which even might be extended for solutions bypassing the bifurcation according to the orientation of the odd branch (Fig. 6).

11. The predicted nominal configuration for a maximum translational working range agrees with the observed leg operation in humans. In Fig. 12A,B, the translational working range is depicted for a human-like segment leg design 2:5:5 depending on the chosen nominal angle configuration and for exponents $\nu = 1, 2$. The working range is largely increased for asymmetric nominal angle configurations. For a nonlinear torque characteristic $(\nu = 2)$ an optimum in working range occurs at $\varphi_{12}^0 \approx 120°$ and $\varphi_{23}^0 \approx 155°$. Note that for the symmetrical axis the working range can be determined analytically (E3).

12. The working range can be further increased by stiffness adjustment. The calculated values for R_C (Fig. 12C,D) correspond to the identified bifurcation. Similar to the observations in Fig. 3C, we can either shift the nominal angles to a more extended knee position for a constant R_C or, vice versa, we can reduce

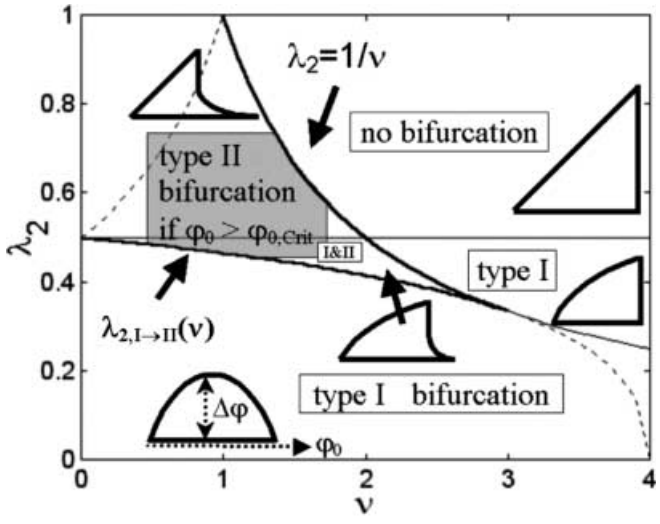

Fig. 9. Regions in (λ_2, ν)-space of different bifurcation behaviour in symmetrical loading. A type I bifurcation is present for $\lambda_2 < 1/2$ and any nominal angle φ_0. The type II bifurcation exists if solutions for φ_B according to the upper extreme $\cos(\varphi_{B,Extr}) = A - \sqrt{B}$ (Fig. 4A,B; Eq. E5) and the corresponding nominal angles φ_0 are within [0, 180°]. With respect to the angular working range $\Delta\varphi(\varphi_0) = \varphi_0 - \varphi_B$ (represented by schematic sketches), the following statements can be made: (i) for $\lambda_2 < 1/2$ the working range is reduced for all nominal angles φ_0 due to type I bifurcation. This leads to a curved graph in $\Delta\varphi(\varphi_0)$; (ii) for $\lambda_2 \geq 1/2$ the working range $\Delta\varphi$ is identical to φ_0 as long as no type II bifurcation appears; (iii) in a region within $\lambda_{2,I\to II}(\nu) < \lambda_2 < 1/\nu$ a sudden decrease in angular working range occurs (Fig. 11) if φ_0 exceeds the critical nominal angle $\varphi_{0,Crit}(\lambda_2, \nu)$ (Fig. 8B) which corresponds to a $\varphi_{B,Extr}$ (Fig. 8D) with $\cos(\varphi_{B,Extr}) = A - \sqrt{B}$ according to (E5). For $\nu < 1$ there is a lower extreme $\cos(\varphi_{B,Extr}) = A + \sqrt{B}$ with $\varphi_B > \varphi_0$ (Fig. 8A,C) if λ_2 exceeds the dashed line $\lambda_2 = 1/(2-\nu)$. For $\nu > 3$ the dashed $\lambda_{2,I\to II}(\nu)$ line (fulfilling $B = 0$) has no importance any more as there is no corresponding bifurcation angle ($A + \sqrt{B} < -1$; Fig. 8C)

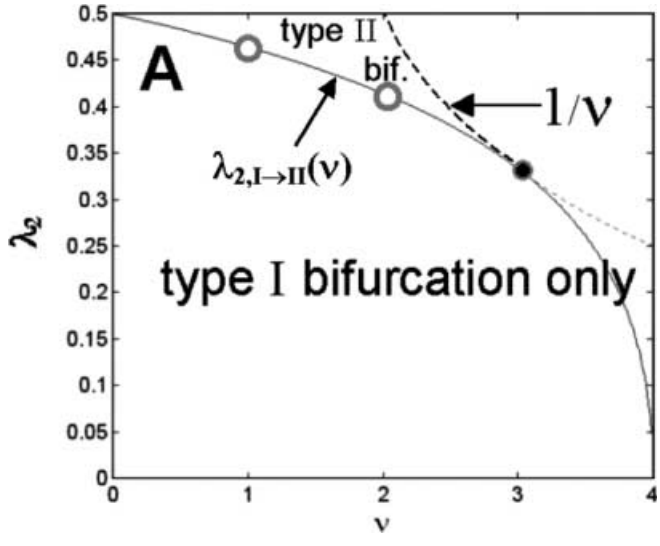

Fig. 10. Critical $\lambda_{2,I\to II}(\nu)$, where for $\nu < 3$ a new type II bifurcation occurs (*small circles* correspond to Fig. 4A,B). An increase in ν from 0 to 3 leads to smaller $\lambda_{2,I\to II}$. For $\nu > 3$, the importance of $\lambda_{2,I\to II}(\nu)$ vanishes as the critical nominal angle leaves the considered interval [0, 180°]. For $3 < \nu \leq 4$, no type II bifurcations occur for λ_2 above $\lambda_{2,I\to II}$ (*solid line*; Fig. 8B,D)

Table 2. Symmetrical loading. Critical relative length of the middle segment $\lambda_{2,I\to II}(\nu)$ (E6) for given exponents of the torque characteristics ν, where for $\lambda_2 \geq \lambda_{2,I\to II}$ a new type II bifurcation appears (Figs. 9 and 10) if the nominal angle φ_0 exceeds a critical nominal angle $\varphi_{0,Crit}(\lambda_2,\nu)$ (here denoted for $\lambda_2 = \lambda_{2,I\to II}$). This critical nominal angle $\varphi_{0,Crit}$ corresponds to the bifurcation angle $\varphi_{B,Crit}$ (denoted again for $\lambda_2 = \lambda_{2,I\to II}$)

ν	$\lambda_{2,I\to II}(\nu)$	$\varphi_{B,Crit}(\lambda_{2,I\to II},\nu)$	$\varphi_{0,Crit}(\varphi_{B,Crit})$
0.5	0.483	36.7°	100.8°
1.0	0.464	54.7°	135.8°
1.5	0.442	71.6°	157.5°
2.0	0.414	90.0°	171.0°
2.5	0.380	114.1°	178.2°

R_C compared to the predicted value for a bifurcation for a constant nominal angle configuration. For example, the optimal working range with $\nu = 2$ predicts a R_C adjustment of about 0.8. As seen in Fig. 3C, we can extend the working range even more by bypassing the bifurcation on the stable side. However, reducing R_C should be limited due to the increase of the magnitude of ankle flexion compared to knee flexion.

13. A nonlinear torque characteristic reduces the asymmetry in joint angles while loading (Fig. 12E,F). As already indicated by Fig. 3B,C, the parallel alignment of the solutions for $Q = 0$ with the symmetrical axis is supported by a nonlinear exponent of the torque characteristic. In Fig. 12 this behaviour is investigated in detail by calculating the position of the bifurcation (φ_{12}^B, φ_{23}^B) relative to various nominal configurations (φ_{12}^0, φ_{23}^0) for $\nu = 1, 2$. The relative location to each other is illustrated in Fig. 12E,F in terms of an inclination angle α representing the ratio of ankle to knee flexion $R_{\Delta\varphi}$. At the symmetrical axis this angle amounts to 45°; i.e., both joint flexions until bifurcation are identical. In the case of linear torque characteristics, small deviations of the nominal configuration from the symmetrical axis lead to an increase in the asymmetry of both joints for knee and ankle angles higher than about 100°. The opposite is true for the nonlinear case. Here the system tends to reduce the asymmetry reaching the bifurcation.

4 Discussion

The kinematic redundancy problem of a three-segment leg (with foot, shank, and thigh) can be solved successfully if quasi-elastic torque characteristics are present at the joints (ankle and knee). The requirements for the joint torque characteristics and the leg geometry were identified.

4.1 Leg design for stable operation

Two different types of leg bending were found: (i) zigzag loading where both joints are flexed simultaneously, or (ii) bow-like loading where both joints tend to stay at the same side with respect to the leg axis.

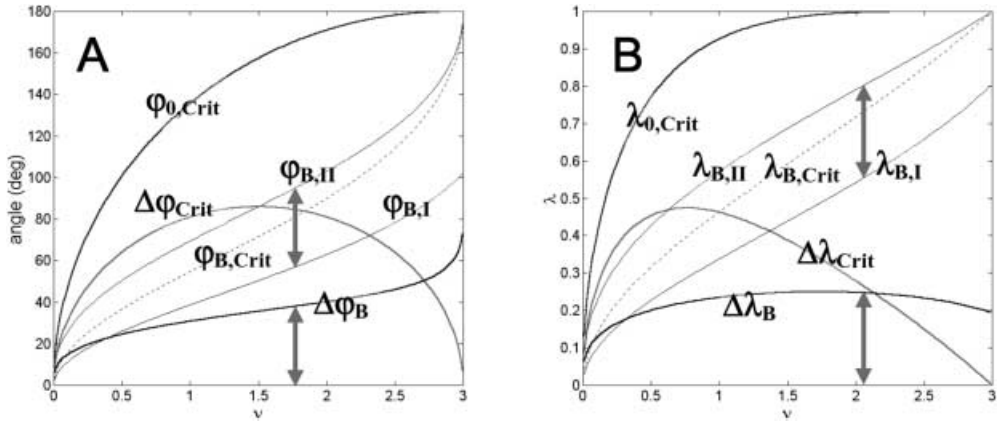

Fig. 11A,B. Further decrease in working range at the transition from type I to type II bifurcation in symmetrical loading (Figs. 9, 10): (**A**) corresponding nominal angle $\varphi_{0,\mathrm{Crit}}$ and bifurcation angle $\varphi_{\mathrm{B,Crit}}$ resulting in an angular working range $\Delta\varphi_{\mathrm{Crit}} = \varphi_{0,\mathrm{Crit}} - \varphi_{\mathrm{B,Crit}}$ for $\lambda_2 = \lambda_{2,\mathrm{I}\to\mathrm{II}}(\nu)$; and **B** relative nominal leg length $\lambda_{0,\mathrm{Crit}}(\varphi_{0,\mathrm{Crit}})$, relative bifurcation length $\lambda_{\mathrm{B,Crit}}(\varphi_{\mathrm{B,Crit}})$, and corresponding relative working range $\Delta\lambda_{\mathrm{Crit}} = \lambda_{0,\mathrm{Crit}} - \lambda_{\mathrm{B,Crit}}$. An increase in ν from 0 to 3 leads to higher $\varphi_{0,\mathrm{Crit}}(\lambda_{2,\mathrm{I}\to\mathrm{II}})$ (**A**). For a satisfactory working range, choosing the exponent ν is important. If a critical nominal angle $\varphi_{0,\mathrm{Crit}}(\nu)$ (Table 2, Fig. 4A,B) is exceeded a sudden decrease in (angular or translational) working range occurs at $\lambda_{2,\mathrm{I}\to\mathrm{II}}(\nu)$ due to the inserted type II bifurcation. This is shown in (**A**, **B**) by $\Delta\varphi_{\mathrm{B}} = \varphi_{\mathrm{B,II}} - \varphi_{\mathrm{B,I}}$ and $\Delta\lambda_{\mathrm{B}} = \lambda_{\mathrm{B,II}} - \lambda_{\mathrm{B,I}}$, respectively ($I$ = type I bifurcation, II = inserted type II bifurcation; a change in φ_0 of 1.8° is considered between I and II)

Leg loading starting with nominal conditions in the zigzag mode as observed in humans and many other mammals may lead to a homogeneous joint flexion for properly adjusted rotational stiffnesses. Considerable adjustment errors result in unequal joint loading and in the worst case lead to leaving the zigzag mode. But even when starting at a symmetrical nominal configuration and keeping the stiffness ratio optimal, the system may lose the symmetry due to stability issues.

Three major segment length design strategies could be identified (Fig. 7): the λ_2 design, the R_λ design, and the design of the $h = 0$ lines. For symmetrical loading the middle segment length design (λ_2 properly adjusted to the exponent ν of the torque characteristic) largely determines the working range.

The ratio of the outer segment lengths R_λ predicts the stiffness adjustment for symmetrical loading but has no influence on the symmetrical working range. Finally, the design of the $h = 0$ lines (Fig. 7B) determines which nominal angles can be used to avoid the attraction of a focus with the consequence of leaving the zigzag mode.

The risk of swapping into the bow mode can be avoided by either low nominal angles or small outer segment lengths shifting the $h = 0$ lines outside the configuration space. A third strategy is the increase of the exponent of the torque characteristics. A fourth possibility is to add elastically operating structures spanning more than one joint.

Making the middle segment (shank) longer than both of the remaining segments (foot and thigh) together ($\lambda_2 > 1/2$) results in avoidance of this unfavourable transition in most cases. But even then the system may yield a bifurcation (type II) for certain nominal angles (Fig. 8B) and exponents of the torque characteristic (Fig. 9). Moreover, a very long middle segment reduces the capability of leg shortening due to geometrical constraints. This solution was not chosen by nature. Middle segment lengths of less than half the total leg length are typical. Then, the range of quasi-symmetric leg shortening (i.e., the working range) is always limited. To reach an optimum angular or translational working range, relative middle segment lengths higher than 0.4 and exponents of the torque characteristic larger than one are necessary (Fig. 5).

4.2 Significance for human legs

In a human leg the relative length of the middle segment (shank) is approximately $\lambda_2 = 0.42$. This is about the region where the inserted type II bifurcation threatens to reduce the working range dramatically for exponent ν values between 1 and 2 (Fig. 11A,B). Increasing the exponent ν the type II bifurcation (Figs. 4, 10) occurs even at smaller middle segment lengths (for $\nu = 2$: $\lambda_{2,\mathrm{I}\to\mathrm{II}} = 0.414$; Table 2). Fortunately, here the critical nominal angle is shifted to almost stretched angle positions (for $\nu = 2$: $\varphi_{0,\mathrm{Crit}} = 171°$; Table 2) and is in general avoided by a more flexed leg at touchdown.

In fact, the human leg design seems to result in a maximum working range for exponent ν values between 1 and 2. Such values correspond to torque characteristics predicted for highly loaded muscle-tendon complexes in the human leg and are mainly determined by tendon stress-strain properties (Seyfarth et al. 2000).

A longer middle segment (or a shorter foot, see Sect. 4.5) would run the risk of a sudden loss in working range for stretched nominal angles (type II bifurcation). Shortening the middle segment or having exponent values smaller than one would clearly reduce the working range (Fig. 5). The asymmetry in the outer segment lengths in a human-like leg resulted in shifted nominal angle configurations for optimum working range. The predicted angle configurations agree with landing conditions in running and hopping (Farley et al. 1998), if an

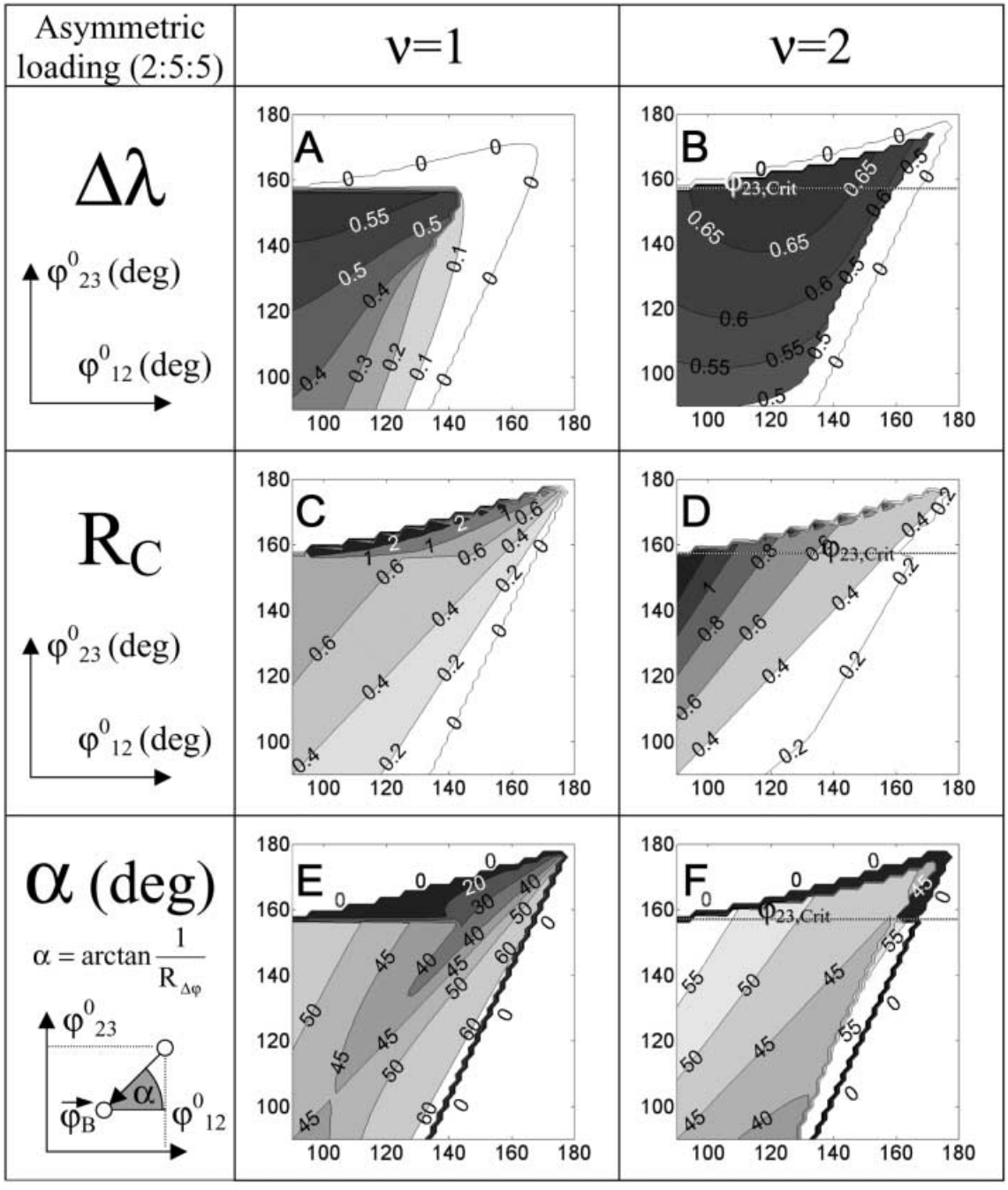

Fig. 12A–F. Asymmetric loading. Influence of the nominal angle configuration (φ_{12}^0, φ_{23}^0) on ($\mathbf{A}, \mathbf{B}$) the maximum translational working range $\Delta\lambda$, ($\mathbf{C}, \mathbf{D}$) the corresponding stiffness adjustment R_C, and ($\mathbf{E}, \mathbf{F}$) the ratio of joint flexions $R_{\Delta\varphi} = (\varphi_{12}^0 - \varphi_{12}^B)/(\varphi_{23}^0 - \varphi_{23}^B)$ expressed as an angle α for a human-like leg design 2:5:5 ($\lambda_2 = 5/12$, $R_\lambda = 2/5$). The location of the bifurcation (φ_{12}^B, φ_{12}^B) nearest to the nominal configuration and R_C are calculated using (7) and (E1)

exponent of the torque characteristic of $v = 2$ is assumed (Fig. 12B: $\varphi_{12}^0 \approx 120°$, $\varphi_{23}^0 \approx 155°$).

4.3 Advantages of operating asymmetrically

The ratio of the outer segment lengths R_λ had no influence on the working range as long as the joints were working in parallel; i.e., the same inner joint angles were present at the ankle and knee joints. Such a symmetrical operation of the leg is achieved by adapting the joint stiffnesses to the length of the adjacent outer segments (stiffness equilibrium, Eqs. 14, 15) and choosing exactly equal nominal angles.

Leaving the symmetrical axis within the configuration space, different outer segment lengths ($R_\lambda \neq 1$) were of advantage. For instance, a small foot (see Sect. 4.5) extended the working range for more stretched nominal knee angles, almost independently of the chosen exponent of the torque characteristic. Thus,

unequal nominal angles and nonlinear torque characteristics are alternative strategies for stable leg operation. Furthermore, the location of the $h_3 = 0$ line where the knee is crossing the leg axis is shifted to high knee angles (Fig. 2B, Table 1), and it allows access to almost the whole upper half of the configuration space ($\varphi_{12} > \varphi_{23}$). Finally, the attraction of the $h = 0$ lines is reduced using higher exponent values of the torque equilibrium (e.g., $\nu = 2$; Fig. 12E,F).

An asymmetrically operating leg with one joint more flexed than the other is advantageous if the outer segment length design is asymmetric. A homogeneous flexion of both joints is then achieved by adapting the stiffness ratio R_C to the chosen difference in nominal angles (Fig. 12C,D). The predicted stiffness adjustment R_C (leading to a bifurcation) is only one strategy to guarantee the denoted working range, other values even might be more advantageous (Figs. 3B–D). This remains to be investigated in more detail.

4.4 The role of biarticular muscles

A homogeneous joint loading is supported by biarticular structures in the leg. Different moment arms of biarticular muscles crossing the knee and ankle joints could help to fulfil the required stiffness ratio. An optimal ratio of the moment arms was found for maximum vertical jumping performance (Fig. 2 in Bobbert and van Zandwijk 1994). Position-dependent moment arms might adapt the ratio to different nominal positions.

As shown in Fig. 3D, only one such muscle (like the gastrocnemius muscle) is necessary to synchronize ankle and knee flexion, as only the upper half of the configuration space is of practical interest. A biarticular antagonist is not required. This coincides with the observation that no such muscle opposite to the gastrocnemius muscle is present in many mammals and humans. The mechanism of the biarticular muscle characterized by the stiffness c_{13} can be described as an effective enhancement of the critical knee angle $\varphi_{23,\mathrm{Crit}}$. In contrast to the case of merely monoarticular springs, the crossing with the $h_3 = 0$ line occurs for nominal angles φ_{23}^0 which are now higher than the intersection itself (Fig. 3D).

4.5 The role of the foot

The introduction of a third leg segment has two major advantages: it reduces the torques required at the leg joints and minimises the energy due to segment rotation (Alexander 1995). The foot length design is critical with respect to the range of safe leg operation. Having a small foot compared to the shank length allows large knee extensions. A small foot compared to the thigh requires a reduced stiffness in the ankle joint with respect to the knee. This requires smaller calf muscle cross-sections compared to the knee extensors, and fits to the generally observed leg design with lower masses at the more distal segments.

Nonetheless, very short feet increase the tendency to snap from the zigzag mode into the bow mode due to the now almost two-segment system. The effective length of the human foot may vary between about 8 and 20 cm, changing the point of support from heel to ball. This results in a relative length of the middle segment near to the type II bifurcation. Two mechanisms are involved to avoid the potential instability:

1. Overextension of the ankle joint is prevented by an increase in effective foot length as the center of pressure is shifted to the tip of the foot. Then, the range of safe leg operation is increased due to a decrease in effective length of the middle segment.
2. Overextension of the knee is avoided by an almost flat touchdown orientation of the foot and the kinematic constraint due to the heel contact. Therefore, the stiffness of the contacting heel pad must be high enough to avoid large deformations which in turn would allow knee overextension. In effect, deformations of about 1 cm are allowed due to the highly nonlinear force-displacement characteristic of the human heel pad (Denoth 1986). This corresponds to a complete leg extension starting at initial knee angles of about 165°.

4.6 Influence of segment masses

The presented model is not able to predict a first impact peak after touchdown (observed, for example, in long jump) even by representing the heel pad by external torques (M_{01}) and replacing the torque characteristics by muscle tendon complexes (Seyfarth et al. 2000). This phenomenon requires the representation of leg segment masses (Denoth 1986). As shown by Gruber (Gruber 1987; Gruber et al. 1998), the proper representation of soft and rigid parts in the human leg is necessary to estimate the internal loads and to predict the observed ground reaction forces. As the leg masses must be decelerated after touchdown, the separation into soft and rigid subsystems allows small foot displacements by reducing the effective mass of the leg (Denoth 1986). The main part of the leg consists of softly coupled masses (Gruber et al. 1998; Seyfarth et al. 1999) whose deceleration is delayed relative to the skeleton. After the impact, the forces predicted by the three-segment model are in agreement with experimental observations for fast types of locomotion (e.g., running and long jump).

Due to neglecting segment masses, zero ground reaction forces during touchdown and take off are requiring zero joint torques at these instants. Therefore, effective joint torques just before landing due to muscular preactivation can not be described adequately with the present three-segment model.

4.7 The leg as a spring?

In this study an elastic joint operation is shown to result in relatively simple strategies for successful leg operation. Nevertheless, there are no structures in the human leg which are compliant enough to account for the observed joint behaviour. Taking the basic muscle

properties (force-length and force-velocity relationships, and activation dynamics) into account the spring-like leg behaviour may result from muscle stimulation optimized for performance. This leads to torque characteristics similar to the results from inverse dynamics (Stefanyshyn and Nigg 1998), and agrees with the assumptions made in this study. The homogeneous loading of the leg joints enables the contribution of the major leg muscles to performance. The sensory control of the leg muscles results in stiffness ratios similar to the values predicted by the three-segment model and in a high leg stiffness at quasi-symmetric leg operation.

The subtle interplay between rotational stiffnesses and the leg stiffness requires further investigation. Nevertheless, the linear spring characteristic observed in biological legs is clearly superior to linear rotational springs, and can be supported by nonlinear tendon properties with exponent values between 1.7 and 2 (Seyfarth et al. 2000). Such values are sufficient for safe leg operation and show the highest advantage in working range for preventing type II bifurcations. Higher exponents would lead to nonlinear leg stiffness behaviour and higher joint loading rates. The latter effect increases the demands on material design. Furthermore, a more sensitive stiffness adjustment to differences in joint angles would be necessary, which requires stiffer ankle joint actuators (Fig. 12C,D).

4.8 Further steps

The strategies developed in this study are suitable for testing in mammalian and human locomotion. First attempts showed promising predictions of leg kinematics for running and jumping. In forward dynamic modeling the effects of heel strike (geometrical constraints at ground support) or changing nominal angles (to represent energy changes as in drop jump or squat jumps) can be considered. The latter effect would help in the neurophysiological understanding of the adjustment of muscle stiffness and rest length (Feldman 1966).

Taking the three-segment model as a starting point, further effects can be taken into account, such as: (a) the influence of additional leg segments, (b) the influence of segment masses and inertias, or (c) the influence of dissipative joint operation (muscles, and heel pad deformation). For (a), the torque equilibrium (2a–c) must be extended by introducing equations representing the additional segments (Appendices A–C). For (b) and (c), the joint variables must be integrated using the differential equations which are replacing the corresponding algebraic equations in the torque equilibrium. The influence of external torques (M_{01}) and moments of inertia (e.g., Θ_3, see Appendix A) can be estimated by taking peak values as a constant in the torque equilibrium. A first estimation of torques M_{01} induced by heel strikes in human revealed that the solutions of the torque equilibrium are only slightly shifted with respect to solutions with $M_{01} = 0$. This remains to be investigated in the future.

Acknowledgements. This research was supported by the German Science Foundation (DFG) within the program 'Autonomes Laufen' (BL236/8–1, WA1420/1–2) and within the program BL236/7. We thank Dr. Sergio Leseduarte for helpful comments on the analysis of the mechanical stability.

Appendix A: General dynamics of a chain of rigid segments

To derive the equations determining the static configuration of the three leg segments in the sagittal plane, we start with the equations of motion of n free rigid bodies ($i = 1, 2, \ldots, n$) in the inertial system:

$$m_i \ddot{\mathbf{r}}_i = \sum_{k(i)} \mathbf{F}_{k,i}$$
$$\boldsymbol{\Theta}_i \dot{\boldsymbol{\omega}}_i = \sum_{k(i)} \left(\mathbf{r}_i + \mathbf{d}_{i,k}\right) \times \mathbf{F}_{k,i} + \sum_{j(i)} \mathbf{M}_{j,i} \quad . \tag{A1a,b}$$

Here the index $k(i)$ denotes the points of interaction with all forces $\mathbf{F}_{k,i}$ working on body i (mass: m_i; moment of inertia tensor $\boldsymbol{\Theta}_i$), whereas $\ddot{\mathbf{r}}_i$ is the acceleration vector of the center of mass (COM) and $\dot{\boldsymbol{\omega}}_i$ is the rotational acceleration with respect to the inertial system. The force $\mathbf{F}_{k,i}$ is acting in a distance $\mathbf{d}_{i,k}$ from the COM. All additional torques (e.g., joint torques) are denoted by $\mathbf{M}_{j,i}$. The dynamics of a chain of n rigid bodies connected by $n - 1$ spherical joints additionally requires the following constraint equations ($i = 1, 2, \ldots, n - 1$):

$$\mathbf{r}_i + \mathbf{d}_{i,i+1} = \mathbf{r}_{i+1} + \mathbf{d}_{i+1,i}$$
$$\mathbf{r}_0 = \mathbf{r}_1 + \mathbf{d}_{1,0} \quad . \tag{A2a,b}$$

For instance, the vector $\mathbf{d}_{2,3}$ points from the COM of body 2 to the joint between the bodies 2 and 3, whereas $\mathbf{d}_{3,2}$ points from the COM of body 3 to the very same joint. Note that $\mathbf{d}_{1,0}$ (A2b) is the distance between the COM of body 1 and the point of application of the ground reaction force.

Let us consider a distal (lower) and a proximal (upper) joint for each body i (or segment i). Taking the gravitational acceleration vector $\mathbf{g}$ into account, (A1) can be written as:

$$m_i \ddot{\mathbf{r}}_i = \mathbf{F}_{i-1,i} + \mathbf{F}_{i+1,i} + m_i \mathbf{g}$$
$$\boldsymbol{\Theta}_i \dot{\boldsymbol{\omega}}_i = \left(\mathbf{r}_i + \mathbf{d}_{i,i-1}\right) \times \mathbf{F}_{i-1,i} + \left(\mathbf{r}_i + \mathbf{d}_{i,i+1}\right) \times \mathbf{F}_{i+1,i} + \mathbf{M}_{i-1,i} + \mathbf{M}_{i+1,i} \quad . \tag{A3a,b}$$

Except for gravity, ground reaction force $\mathbf{F}_{0,1}$, and ground torque $\mathbf{M}_{0,1}$, all forces and torques are internal. For instance, at the joint between bodies 2 and 3, $\mathbf{F}_{3,2}$ and $\mathbf{M}_{3,2}$ are the constraint force and the torque (produced by structures spanning the very same joint) acting on body 2. The corresponding force $\mathbf{F}_{2,3}$ and torque $\mathbf{M}_{2,3}$ are pointing in the opposite direction and are acting on body 3, or generally:

$$\mathbf{F}_{i+1,i} = -\mathbf{F}_{i,i+1}$$
$$\mathbf{M}_{i+1,i} = -\mathbf{M}_{i,i+1} \quad . \tag{A4a,b}$$

Appendix B: Segment dynamics neglecting inertial contributions (m_i, Θ_i) of the leg

The dynamic properties of a segment (body i) will be neglected by setting its mass m_i and moment of inertia $\mathbf{\Theta}_i$ to zero. This is the case for all leg segments ($i = 1, 2, 3$). Furthermore, all body weight is shifted to the uppermost segment (body 4). Later, even the moment of inertia of this remaining mass will be neglected.

The assumption of a quasi-static operation of the leg in the system (A3a) together with (A4a) leads to ($i = 1, 2, \ldots, n-1$):

$$\mathbf{F}_{0,1} = \mathbf{F}_{i,i+1} = -\mathbf{F}_{i+1,i} \ . \tag{B1}$$

For a massless leg (segments $i = 1, 2, 3$) supporting a mass (body 4) at the proximal end of the third leg segment and touching the ground at its distal end (segment 1), we can reduce the system (A3a,b) to a planar model ($i = 1, 2, 3$):

$$\begin{aligned}
&\left[\left(\mathbf{d}_{i,i+1} - \mathbf{d}_{i,i-1}\right) \times \mathbf{F}_{0,1}\right]\big|_z = \mathbf{M}_{i-1,i}|_z - \mathbf{M}_{i,i+1}|_z \\
&m_4 \ddot{\mathbf{r}}_4 = \mathbf{F}_{0,1} + m_4 \mathbf{g} \\
&\Theta_4 \ddot{\varphi}_4 = \left[\left(\mathbf{r}_4 + \mathbf{d}_{4,3}\right) \times \mathbf{F}_{0,1}\right]\big|_z + \mathbf{M}_{3,4}|_z
\end{aligned} \tag{B2a–c}$$

where Θ_4 is the principal moment of inertia of body 4 with respect to z. For each leg segment (B2a) there remains only one equation determining the torque equilibrium. Additionally, we have two equations (B2b) describing the translational acceleration and one equation (B2c) representing the rotational acceleration of the supported body ($i = 4$). Note that all torques are pointing into the z-direction, perpendicular to the sagittal plane.

Appendix C: Reduction to a point mass model ($\Theta_4 = 0$)

In order to describe the total body COM dynamics in terms of a point mass, the supported segment has to be reduced to zero length ($d_{4,3} = |\mathbf{d}_{4,3}| = 0$) and zero moment of inertia ($\Theta_4 = 0$). Consequently, there can not be a torque acting on the supported mass ($M_{34} = \mathbf{M}_{3,4}|_z = 0$) which leads to:

$$\begin{aligned}
&m\ddot{\mathbf{r}} = \mathbf{F}_{\text{leg}} + m\mathbf{g} \\
&\left(\mathbf{l}_1 \times \mathbf{F}_{\text{leg}}\right)\big|_z = M_{01} - M_{12} \\
&\left(\mathbf{l}_2 \times \mathbf{F}_{\text{leg}}\right)\big|_z = M_{12} - M_{23} \\
&\left(\mathbf{l}_3 \times \mathbf{F}_{\text{leg}}\right)\big|_z = M_{23} \\
&\mathbf{r} = \mathbf{l}_1 + \mathbf{l}_2 + \mathbf{l}_3
\end{aligned} \tag{C1a–e}$$

with $\mathbf{l}_i = \mathbf{d}_{i,i+1} - \mathbf{d}_{i,i-1}$, $\mathbf{F}_{\text{leg}} = \mathbf{F}_{0,1}$, $m = m_4$, and $\mathbf{r} = \mathbf{r}_4 - \mathbf{r}_0$. For simplicity, M_{ji} denotes $\mathbf{M}_{j,i}|_z$. The last equation (C1e) follows directly from (A2) by subsequently subtracting (A2a) with $i = 1, 2, 3$ from (A2b). With given torques M_{01}, M_{12} and M_{23} as functions of the leg configuration φ_1, φ_2 and φ_3, one can solve the system (C1b–e) of five equations for the five unknowns φ_1, φ_2, φ_3, $F_{\text{leg},x}$ and $F_{\text{leg},y}$ at any point in time.

For *forward dynamic integration* of (C1a), an initial configuration φ_1, φ_2 and φ_3 must be chosen which fulfils the system (C1b–e) in accordance to the torque characteristics $M_{ij}(\varphi_1, \varphi_2, \varphi_3)$. For example, using rotational springs (12a,b), this can easily be realized by setting the initial angles to the nominal angles. Then by solving the system (C1b–e) at each time step, the acting force – and therefore the body mass dynamics – can be calculated.

Appendix D: Stability at solutions for $Q = 0$

To fulfil a stable leg configuration at torque equilibrium (denoted by $Q = 0$; Eqs. 5 and 7) we need to consider the potential energy of the torque actuators at the knee and ankle joints with respect to displacements within the internal joint configurations at a given leg length r. Nearby $Q = 0$ we can approximate E and r until the second order:

$$\begin{aligned}
E(\boldsymbol{\varphi}) = {} & E(\boldsymbol{\varphi}_{Q=0}) + \nabla_{\boldsymbol{\varphi}} E(\boldsymbol{\varphi}_{Q=0}) \cdot \Delta\boldsymbol{\varphi} \\
& + \frac{1}{2} \Delta\boldsymbol{\varphi}^{\mathrm{T}} \cdot \mathbf{H}_E(\boldsymbol{\varphi}_{Q=0}) \cdot \Delta\boldsymbol{\varphi} + \mathrm{o}(\Delta\boldsymbol{\varphi}^3)
\end{aligned} \tag{D1}$$

$$\begin{aligned}
r(\boldsymbol{\varphi}) = {} & r(\boldsymbol{\varphi}_{Q=0}) + \nabla_{\boldsymbol{\varphi}} r(\boldsymbol{\varphi}_{Q=0}) \cdot \Delta\boldsymbol{\varphi} \\
& + \frac{1}{2} \Delta\boldsymbol{\varphi}^{\mathrm{T}} \cdot \mathbf{H}_r(\boldsymbol{\varphi}_{Q=0}) \cdot \Delta\boldsymbol{\varphi} + \mathrm{o}(\Delta\boldsymbol{\varphi}^3)
\end{aligned} \tag{D2}$$

where $\boldsymbol{\varphi}$ denotes the angular configuration ($\varphi_{12}, \varphi_{23}$), $\Delta\boldsymbol{\varphi}$ is the displacement in $\boldsymbol{\varphi}$ and $\mathbf{H}_E$, $\mathbf{H}_r$ are representing the Hessian matrices of the scalar fields E and r containing the second-order derivatives with respect to $\boldsymbol{\varphi}$. For stability we demand $\Delta E = E(\boldsymbol{\varphi}) - E(\boldsymbol{\varphi}_{Q=0}) > 0$ with $\Delta r = r(\boldsymbol{\varphi}) - r(\boldsymbol{\varphi}_{Q=0}) = 0$. The latter equation $\Delta r = 0$ determines all allowed disturbances $\Delta\boldsymbol{\varphi}$ which can be separated ($\Delta\boldsymbol{\varphi} = \Delta\boldsymbol{\varphi}_\perp + \Delta\boldsymbol{\varphi}_\parallel$ where $\Delta\boldsymbol{\varphi}_\perp = \frac{\Delta\boldsymbol{\varphi}\cdot\mathbf{t}_r}{|\mathbf{t}_r|^2}\mathbf{t}_r$, $\Delta\boldsymbol{\varphi}_\parallel = \frac{\Delta\boldsymbol{\varphi}\cdot\nabla_{\boldsymbol{\varphi}} r}{|\nabla_{\boldsymbol{\varphi}} r|^2}\nabla_{\boldsymbol{\varphi}} r$) and with any vector $\mathbf{t}_r$ perpendicular to $\nabla_{\boldsymbol{\varphi}} r$:

$$\begin{aligned}
&\nabla_{\boldsymbol{\varphi}} r(\boldsymbol{\varphi}_{Q=0}) \cdot \Delta\boldsymbol{\varphi}_\parallel \\
&\quad = -\frac{1}{2} \Delta\boldsymbol{\varphi}_\perp^{\mathrm{T}} \cdot \mathbf{H}_r(\boldsymbol{\varphi}_{Q=0}) \cdot \Delta\boldsymbol{\varphi}_\perp + \mathrm{o}(\Delta\boldsymbol{\varphi}^3) \ .
\end{aligned} \tag{D3}$$

Hereby, $\Delta\boldsymbol{\varphi}_\perp \gg \Delta\boldsymbol{\varphi}_\parallel$ is assumed. Substituting (9) and (D3) in (D1) leads to the asked energy fluctuation surrounding $Q = 0$:

$$\Delta E = \frac{1}{2} \left(\frac{\Delta\boldsymbol{\varphi} \cdot \mathbf{t}_r}{|\mathbf{t}_r|^2} \right)^2 \cdot \mathbf{t}_r^{\mathrm{T}} \cdot \Delta\mathbf{H} \cdot \mathbf{t}_r \ , \tag{D4}$$

with

$$\Delta\mathbf{H} = \mathbf{H}_E(\boldsymbol{\varphi}_{Q=0}) + F_{\text{leg}}(\boldsymbol{\varphi}_{Q=0}) \cdot \mathbf{H}_r(\boldsymbol{\varphi}_{Q=0}) \ . \tag{D5}$$

The Hessian matrices are defined as follows:

$$\mathbf{H}_E = \begin{pmatrix} \frac{\partial^2 E}{\partial\varphi_{12}\partial\varphi_{12}} & \frac{\partial^2 E}{\partial\varphi_{12}\partial\varphi_{23}} \\ \frac{\partial^2 E}{\partial\varphi_{23}\partial\varphi_{12}} & \frac{\partial^2 E}{\partial\varphi_{23}\partial\varphi_{23}} \end{pmatrix} = \begin{pmatrix} -\frac{\partial M_{12}}{\partial\varphi_{12}} & -\frac{\partial M_{12}}{\partial\varphi_{23}} \\ \frac{\partial M_{23}}{\partial\varphi_{12}} & \frac{\partial M_{23}}{\partial\varphi_{23}} \end{pmatrix} \tag{D6}$$

and

$$\mathbf{H}_r = \begin{pmatrix} \frac{\partial^2 r}{\partial\varphi_{12}\partial\varphi_{12}} & \frac{\partial^2 r}{\partial\varphi_{12}\partial\varphi_{23}} \\ \frac{\partial^2 r}{\partial\varphi_{23}\partial\varphi_{12}} & \frac{\partial^2 r}{\partial\varphi_{23}\partial\varphi_{23}} \end{pmatrix} = \begin{pmatrix} \frac{\partial h_1}{\partial\varphi_{12}} & \frac{\partial h_1}{\partial\varphi_{23}} \\ \frac{\partial h_3}{\partial\varphi_{12}} & \frac{\partial h_3}{\partial\varphi_{23}} \end{pmatrix} . \tag{D7}$$

For the case of merely monoarticular torque actuators (e.g., Eqs. 12a,b) the matrix $\mathbf{H}_E$ becomes diagonal. Due to the leg length of the three-segment system (3) the Hessian $\mathbf{H}_r$ is symmetrical. Consequently, this results in a symmetrical difference matrix $\mathbf{\Delta H}$.

A stable torque equilibrium is fulfilled if both eigenvalues $w_{1,2}$ of $\mathbf{\Delta H}$ are positive, or more generally if

$$\mathbf{t}_r^{\mathrm{T}} \cdot \mathbf{\Delta H} \cdot \mathbf{t}_r = w_1 \cdot t_1^2 \cdot |\mathbf{e}_1|^2 + w_2 \cdot t_2^2 \cdot |\mathbf{e}_2|^2 > 0 \tag{D8}$$

where $\mathbf{t}_r = t_1 \cdot \mathbf{e}_1 + t_2 \cdot \mathbf{e}_2$ and $\mathbf{e}_{1,2}$ are the eigenvectors of $\mathbf{\Delta H}$.

Due to the equivalence of $\nabla_{\boldsymbol{\varphi}} Q = \mathbf{\Delta H} \cdot \mathbf{t}_r$ derived using (4), (5), (D5) and $\mathbf{t}_r = \begin{pmatrix} -h_3 \\ h_1 \end{pmatrix}$, we can distinguish two possibilities for $\mathbf{t}_r^{\mathrm{T}} \cdot \mathbf{\Delta H} \cdot \mathbf{t}_r = 0$, see (D4) i.e., for the transition from stability to instability:

1. $\nabla_{\boldsymbol{\varphi}} Q = 0$; i.e., the condition for a bifurcation (see Appendix E) which requires $\det(\mathbf{\Delta H}) = 0$ and $\mathbf{t}_r$ is an eigenvector corresponding to the vanishing eigenvalue, or
2. $\nabla_{\boldsymbol{\varphi}} Q \| \nabla_{\boldsymbol{\varphi}} r$; i.e., the solution for $Q = 0$ aligns with an $r = const.$ line (Fig. 6).

Appendix E: Conditions for the bifurcation point

In the case of symmetrical nominal angle configuration $\varphi_0 = \varphi_{12}^0 = \varphi_{23}^0$, the stiffness equilibrium ($R_C = R_\lambda$) leads to a symmetrical solution ($\varphi_{12} = \varphi_{23}$) of the torque equilibrium (5, 7), which might be crossed by an odd solution. The intersectional point between these solutions of $Q(\varphi_{12}, \varphi_{23}) = 0$ is called a bifurcation point, which is determined by the condition $\nabla_{\boldsymbol{\varphi}} Q(\varphi_{12}, \varphi_{23}) = 0$. It represents a saddle point of the Q function within the configuration space. The components of the gradient can be expressed for the three segment system as:

$$\begin{aligned} \frac{\partial Q}{\partial\varphi_{12}} &= \lambda_1 \cos\varphi_{12} \cdot M_{23} + \lambda_3 \sin\varphi_{23} \frac{\partial M_{12}}{\partial\varphi_{12}} \\ &\quad + \frac{\lambda_1\lambda_3}{\lambda_2} \left[\frac{\partial M_{12}}{\partial\varphi_{12}} \sin(\varphi_{12} - \varphi_{23}) \right. \\ &\quad \left. + (M_{12} - M_{23}) \cos(\varphi_{12} - \varphi_{23}) \right] = 0 \\ \frac{\partial Q}{\partial\varphi_{23}} &= \lambda_3 \cos\varphi_{23} \cdot M_{12} + \lambda_1 \sin\varphi_{12} \frac{\partial M_{23}}{\partial\varphi_{23}} \\ &\quad - \frac{\lambda_1\lambda_3}{\lambda_2} \left[\frac{\partial M_{23}}{\partial\varphi_{23}} \sin(\varphi_{12} - \varphi_{23}) \right. \\ &\quad \left. + (M_{12} - M_{23}) \cos(\varphi_{12} - \varphi_{23}) \right] = 0 \end{aligned} \tag{E1a,b}$$

In general a bifurcation can be found in an asymmetric nominal angle configuration if R_C is properly adapted. Therefore, the solutions of $\nabla_{\boldsymbol{\varphi}} Q(\varphi_{12}, \varphi_{23}) = 0$ together with $Q(\varphi_{12}, \varphi_{23}) = 0$ do not merely provide the bifurcation point $\varphi_{\mathrm{B},12}$, $\varphi_{\mathrm{B},23}$ but also the corresponding stiffness ratio R_C.

For symmetrical loading ($\varphi = \varphi_{12} = \varphi_{23}$, with $\varphi_0 = \varphi_{12}^0 = \varphi_{23}^0$ and $R_C = R_\lambda$) the two equations for the condition $\nabla_{\boldsymbol{\varphi}} Q(\varphi_{12}, \varphi_{23}) = 0$ (E1a,b) become linearly dependent and can therefore be simplified to one equation. In the case of rotational springs at the joints (12a,b), this leads to:

$$\begin{aligned} &\nu \sin\varphi \cdot (\varphi_0 - \varphi)^{\nu-1} \\ &\quad + \left(\cos\varphi - \frac{\lambda_1 + \lambda_3}{\lambda_2} \right) \cdot (\varphi_0 - \varphi)^{\nu} = 0 . \end{aligned} \tag{E2}$$

For $\varphi \neq \varphi_0$ this explicitly defines the nominal angle φ_0 as a function of the bifurcation angle φ_{B}, the relative length of the middle segment λ_2, and the exponent ν of the torque characteristic:

$$\varphi_0(\varphi_{\mathrm{B}}) = \frac{\nu \sin\varphi_{\mathrm{B}}}{\Lambda_2 - \cos\varphi_{\mathrm{B}}} + \varphi_{\mathrm{B}} \tag{E3}$$

with $\Lambda_2 = (1 - \lambda_2)/\lambda_2$. This function implicitly defines all bifurcations φ_{B} that are present for a given nominal angle φ_0 (Fig. 4). For $\lambda_2 < 1/2$ there is always at least one bifurcation. For $\lambda_2 > \lambda_{2,\mathrm{I}\to\mathrm{II}}(\nu)$ there may be additional bifurcations (one or two) if φ_0 is larger than the critical $\varphi_0(\lambda_{2,\mathrm{I}\to\mathrm{II}}(\nu))$. To identify the criteria for multiple bifurcations we consider the local extremes of $\varphi_0(\varphi_{\mathrm{B}})$, which are given by

$$\frac{\partial\varphi_0}{\partial\varphi_{\mathrm{B}}} = \Lambda_2^2 - \nu + \Lambda_2(\nu - 2)\cos\varphi_{\mathrm{B}} + \cos^2\varphi_{\mathrm{B}} = 0 , \tag{E4}$$

yielding the solutions:

$$\begin{aligned} \cos\varphi_{\mathrm{B,Extr}} &= \frac{\Lambda_2(2 - \nu)}{2} \pm \sqrt{\frac{\Lambda_2^2\nu(\nu - 4) + 4\nu}{4}} \\ &= \mathrm{A} \pm \sqrt{\mathrm{B}} . \end{aligned} \tag{E5}$$

The values for $\varphi_{\mathrm{B,Extr}}$ and the corresponding $\varphi_{0,\mathrm{Extr}}$ (E3) are depicted in Fig. 8. Vanishing of the square root defines a condition for a critical $\lambda_{2,\mathrm{I}\to\mathrm{II}}(\nu)$ where additional bifurcations within $0 \le \varphi \le \pi$ may appear (see Fig. 10):

$$\lambda_{2,\mathrm{I}\to\mathrm{II}}(\nu) = \frac{1}{1 + \sqrt{\frac{1}{1 - \nu/4}}} . \tag{E6}$$

Appendix F: Existence and consequences of type II bifurcation

Two conditions are necessary and sufficient for a type II bifurcation:
Condition 1. λ_2 must fulfil $1/\nu > \lambda_2 \ge \lambda_{2,\mathrm{I}\to\mathrm{II}}(\nu)$ (Fig. 9).
Condition 2. the nominal angle φ_0 is greater than an angular threshold $\varphi_{0,\mathrm{Crit}}(\lambda_2, \nu)$ (Fig. 8).

This critical angle $\varphi_{0,\mathrm{Crit}}$ results from $\varphi_0(\varphi_{\mathrm{B}})$ (E3) with $\cos\varphi_{\mathrm{B,Extr}} = \mathrm{A} - \sqrt{\mathrm{B}}$ according to the upper extreme (negative sign in Eq. E5). The condition $\lambda_2 < 1/\nu$ (part of condition 1) is a consequence of (E5) where the right side must be within $[-1, 1]$.

In Fig. 11A and B, the effects of an emerging type II bifurcation (for $\lambda_2 = \lambda_{2,\mathrm{I}\to\mathrm{II}}(v)$) on the angular and translational working range are shown for $0 \leq v \leq 3$. To consider the inset of the type II bifurcation, the corresponding critical nominal angles $\varphi_{0,\mathrm{Crit}}$ (or lengths $\lambda_{0,\mathrm{Crit}}$; Table 2) were depicted.

The working range $\Delta\varphi_{\mathrm{Crit}}$ (or $\Delta\lambda_{\mathrm{Crit}}$, respectively) around such a critical nominal angle (or length) changes dramatically if a nominal angle slightly above or below the critical $\varphi_{0,\mathrm{Crit}}$ is chosen (a change in φ_0 of 1.8° is considered). At $v \approx 1.75$ there is a maximum loss of $\Delta\lambda_{\mathrm{B}} \approx 0.25$ in translational working range $\Delta\lambda$, due to the appearance of the type II bifurcation.

References

Alexander RM (1995) Leg design and jumping technique for humans, other vertebrates and insects. Phil Trans R Soc Lond B Bi Sci 347: 235–248

Bernstein N (1967) The coordination and regulation of movements. Pergamon, Oxford

Blickhan R (1989) The spring-mass model for running and hopping. J Biomech 22: 1217–1227

Bobbert MF, van Zandwijk JP (1994) Dependence of human maximum jump height on moment arms of the biarticular m. gastrocnemius; a simulation study. Hum Mov Sci 13: 697–716

Denoth J (1986) Load on the locomotor system and modelling. In: Nigg BM (ed) Biomechanics of running shoes. Human Kinetics, Champaign, Ill

Dornay M, Mussa-Ivaldi FA, McIntyre J, Bizzi E (1993) Stability constraints for the distributed control of motor behavior. Neural Netw 6: 1045–1059

Farley CT, Morgenroth (1999) Leg stiffness primarily depends on ankle stiffness during human hopping. J Biomech 32: 267–273

Farley CT, González O (1996) Leg stiffness and stride frequency in human running. J Biomech 29: 181–186

Farley CT, Houdijk HHP, van Strien C, Louie M (1998) Mechanisms of leg stiffness adjustment for hopping on surfaces of different stiffnesses. J Appl Physiol 85: 1044–1055

Feldman AG (1966) Functional tuning of the nervous system during control of movement or maintenance of a steady posture. II. Controllable parameters of the muscle. Biophysics 11: 565–578

Gielen CCAM, van Bolhuis BM, Theeuwen M (1995) On the control of biologically and kinematically redundant manipulators. Hum Mov Sci 14: 487–509

Gruber K (1987) Entwicklung eines Modells zur Berechnung der Kräfte im Knie- und Hüftgelenk bei sportlichen Bewegungsabläufen mit hohen Beschleunigungen. Dissertation, Universität Tübingen

Gruber K, Ruder H, Denoth J, Schneider K (1998) A comparative study of impact dynamics: wobbling mass model versus rigid body models. J Biomech 31: 439–444

Kovacs I, Tihanyi J, Devita P, Racz L, Barrier J, Hortobagyi T (1999) Foot placement modifies kinematics and kinetics during drop jumping. Med Sci Sports Exerc 31: 708–716

van Leeuwen JL (1992) Muscle function in locomotion. In: Alexander RM (ed) Mechanics of animal locomotion. (Advances in comparative and environmental physiology, vol 11) Springer, Berlin Heidelberg New York, pp 191–242

Seyfarth A, Friedrichs A, Wank V, Blickhan R (1999) Dynamics of the long jump. J Biomech 32: 1259–1267

Seyfarth A, Blickhan R, van Leeuwen JL (2000) Optimum take-off techniques and muscle design for long jump. J Exp Biol 203: 741–750

Stefanyshyn DJ, Nigg BM (1998) Contribution of the lower extremity to the mechanical energy in running vertical jumps and running long jumps. J Sport Sci 16: 177–186

Wagner H, Blickhan R (1999) Stabilizing function of skeletal muscles: an analytical investigation. J Theor Biol 199: 163–179

Williams KR, Snow R, Agruss C (1991) Changes in distance running kinematics with fatigue. Int J Sport Biomech 7: 138–162

Winters JM (1995) How detailed should muscle models be to understand multi-joint movement coordination? Hum Mov Sci 14: 401–442